REPORT DOCUMENTATION PAGE

Form Approved OMB NO. 0704-0188

1. REPORT DATE (DD-MM-YYYY)	2. REPORT TYPE	3. DATES COVERED (From - To)
21-11-2013	Final Report	1-Jun-2010 - 31-May-2013

4. TITLE AND SUBTITLE
Mechanics of the Adhesive Properties of Ivy Nanoparticles

5a. CONTRACT NUMBER
W911NF-10-1-0114

5b. GRANT NUMBER

5c. PROGRAM ELEMENT NUMBER
611102

6. AUTHORS
Mingjun Zhang

5d. PROJECT NUMBER

5e. TASK NUMBER

5f. WORK UNIT NUMBER

7. PERFORMING ORGANIZATION NAMES AND ADDRESSES
University of Tennessee at Knoxville
Office of Research & Engagement
1534 White Avenue
Knoxville, TN 37996 -1529

8. PERFORMING ORGANIZATION REPORT NUMBER

9. SPONSORING/MONITORING AGENCY NAME(S) AND ADDRESS (ES)
U.S. Army Research Office
P.O. Box 12211
Research Triangle Park, NC 27709-2211

10. SPONSOR/MONITOR'S ACRONYM(S)
ARO

11. SPONSOR/MONITOR'S REPORT NUMBER(S)
56015-LS.40

12. DISTRIBUTION AVAILIBILITY STATEMENT
Approved for Public Release; Distribution Unlimited

13. SUPPLEMENTARY NOTES
The views, opinions and/or findings contained in this report are those of the author(s) and should not contrued as an official Department of the Army position, policy or decision, unless so designated by other documentation.

14. ABSTRACT
The research objective of this proposal is to study the fundamental mechanics and mechanical properties of the nanoparticles-based adhesive secretion produced by ivy rootlets for surface affixing and climbing. Both experimental and theoretical studies will be conducted. More generally, we aim to use insight from nature to elucidate theoretical principles governing the extraordinary adhesive properties of ivy. The specific aims are:

Specific Aim 1: Characterize the intra- and inter- molecular bonding forces and determine how they can be used to

15. SUBJECT TERMS
Ivy high strength adhesive, nanoparticles, bio-inspired adhesive

16. SECURITY CLASSIFICATION OF:			17. LIMITATION OF ABSTRACT	15. NUMBER OF PAGES	19a. NAME OF RESPONSIBLE PERSON
a. REPORT	b. ABSTRACT	c. THIS PAGE			Mingjun Zhang
UU	UU	UU	UU		19b. TELEPHONE NUMBER 865-974-7620

Report Title

Mechanics of the Adhesive Properties of Ivy Nanoparticles

ABSTRACT

The research objective of this proposal is to study the fundamental mechanics and mechanical properties of the nanoparticles-based adhesive secretion produced by ivy rootlets for surface affixing and climbing. Both experimental and theoretical studies will be conducted. More generally, we aim to use insight from nature to elucidate theoretical principles governing the extraordinary adhesive properties of ivy. The specific aims are:

Specific Aim 1: Characterize the intra- and inter- molecular bonding forces and determine how they can be used to explain interactions that exist both between components of the ivy adhesive secretion and between the secretion and the affixing surface.

Specific Aim 2: Characterize the macroscopic mechanical properties of natural ivy secretions.

Specific Aim 3: Determine structure-property relationships via systematic alteration of the composition of the natural ivy secretions.

Specific Aim 4: Build finite element models (FEM) to quantitatively characterize and interpret the adhesive properties of ivy nanoparticles.

If successful, this research will elucidate the fundamental role of nanoparticles in determining the mechanical properties of ivy surface affixing secretions, and will inspire bio-mimetic approaches for design of new materials with superior surface adhesion for military applications.

Enter List of papers submitted or published that acknowledge ARO support from the start of the project to the date of this printing. List the papers, including journal references, in the following categories:

(a) Papers published in peer-reviewed journals (N/A for none)

Received	Paper
02/26/2013 23.00	Jacques E. Abboud, Xinyuan Chong, Mingjun Zhang, Zhili Zhang, Naibo Jiang, Sukesh Roy, James R. Gord. Photothermally Activated Motion and Ignition Using Aluminum Nanoparticles, Applied Phylics letters, (01 2013): 1. doi:
02/26/2013 24.00	Yujian Huang, Scott C Lenaghan, Lijin Xia, Jason N Burris, C Neal Stewart Jr, Mingjun Zhang. Characterization of Physicochemical Properties of Ivy Nanoparticles, Journal of Nanobiotechnology, (12 2012): 0. doi:
02/27/2013 25.00	Yongzhong Wang, Leming Sun, Sijia Yi, Yujian Huang, Scott C. Lenaghan, Mingjun Zhang. Naturally Occurring Nanoparticles from Arthrobotrys oligospora as a Potential Immunostimulatory and Antitumor Agent, Advaced Functional materials , (12 2012): 0. doi:
05/16/2013 31.00	Lijin Xia, Zhonghua Xu, Leming Sun, Patrick M. Caveney, Mingjun Zhang. Nanofillers to Tune the Young's Modulus of Silicone Matrix, Journal of Nanoparticle Research, (03 2013): 1570. doi:
05/16/2013 33.00	Leming Sun, Lijin Xia, Sijia Yi, Scott C. Lenaghan, Yongzhong Wang, Mingjun Zhang. Biosynthesis of gold and silver nanoparticles using vegetable waste from the peel of Asparagus Lettuce (Lactuca sativa var. asparagine), Advanced Science, Engineering and Medicine (ASEM), (03 2013): 0. doi:
05/16/2013 32.00	Sijia Yi, Leming Sun, Scott C. Lenaghan, Yongzhong Wang, Xinyuan Chong, Zhili Zhang, Mingjun Zhang. One-step Synthesis of Dendritic Gold Nanoflowers with High Surface-Enhanced Raman Scattering (SERS), RSC Advances, (06 2013): 0. doi:
06/04/2012 12.00	Pelagie M. Favi, Sijia Yi, Scott C. Lenaghan, Lijin Xia, Mingjun Zhang. Inspiration from the natural world: from bio-adhesives to bio-inspiredadhesives, Journal of Adhesion Science and Technology, (05 2012): 0. doi:
08/20/2012 14.00	Sijia Yi, Scott C. Lenaghan, Mingjun Zhang, Lijin Xia. Facile synthesis of biocompatible gold nanoparticles with organosilicone-coated surface properties, Journal of Nanoparticle Research, (06 2012): 0. doi: 10.1007/s11051-012-0960-z
08/20/2012 17.00	Lijin Xia, Scott C. Lenaghan, Andrew B. Wills, Yinyuan Chen, Mingjun Zhang. Evaluation of the nanofibrillar structure of Dioscorea opposite extract for cell attachment, Colloids and Surfaces B: Biointerfaces, (11 2011): 0. doi: 10.1016/j.colsurfb.2011.07.025
08/20/2012 16.00	Scott C. Lenaghan, Mingjun Zhang. Real-time observation of the secretion of a nanocomposite adhesive from English ivy (Hedera helix), Plant Science, (02 2012): 0. doi: 10.1016/j.plantsci.2011.08.013
08/25/2013 35.00	Scott C. Lenaghan, Jason N. Burris, Karuna Chourey, Yujian Huang, Lijin Xia, Belinda Lady, Ritin Sharma, Chongle Pan, Zorabel LeJeune, Shane Foister, Robert L. Hettich, C. Neal Stewart Jr, Mingjun Zhang. Isolation and Chemical Analysis of Nanoparticles from English Ivy (Hedera helix L.), Journal of the Royal Society Interface, (07 2013): 0. doi:

08/25/2013	38.00	Scott C. Lenaghan, Yuanyuan Li, Hao Zhang, Jason N. Burris, C. Neal Stewart, Jr., Lynne E. Parker, Mingjun Zhang. Monitoring the Environmental Impact of TiO2 Nanoparticles Using a Plant-based Sensor-network, IEEE Transactions on Nanotechnology, (03 2013): 182. doi:
08/25/2013	36.00	Sijia Yi, Yongzhong Wang, Yujian Huang, Lijin Xia, Leming Sun, Scott C. Lenaghan, Mingjun Zhang. Tea Nanoparticles for Immunostimulation andChemo-Drug Delivery in Cancer Treatment, Journal of Biomedical Nanotechnology, (01 2014): 1. doi:
09/09/2010	1.00	Lijin Xia, Scott C Lenaghan, Mingjun Zhang, Zhili Zhang and Quanshui Li. Naturally occurring nanoparticles from English ivy: an alternative to metal-based nanoparticles for UV protection, Journal of Nanobiotechnology, (09 2010): . doi:
12/05/2010	3.00	Lijin Xia • Scott C. Lenaghan • Mingjun Zhang • Yu Wu • Xiaopeng Zhao • Jason N. Burris • C. Neal Stewart Jr.. Characterization of English ivy (Hedera helix) adhesion force and imaging using atomic force microscopy, Journal of Nanoparticle Research, (09 2010): . doi:
12/05/2010	4.00	Lijin Xia, Scott C. Lenaghan and Mingjun Zhang. NATURALLY OCCURING NANOFIBER NETWORK FROM THE SUNDEW FOR TISSUE ENGINEERING, , (12 2010): . doi:
12/05/2010	5.00	Scott C. Lenaghan, Lijin Xia, W.R. Henson, and Mingjun Zhang. ISOLATION AND CHARACTERIZATION OF NANOPARTICLES FROM ENGLISH IVY (HEDERA HELIX), , (12 2010): . doi:
TOTAL:	**17**	

Number of Papers published in peer-reviewed journals:

(b) Papers published in non-peer-reviewed journals (N/A for none)

Received		Paper
08/25/2013	37.00	Mingjun Zhang. Fungus-based nanoparticles: inspiration from naturefor cancer therapy, Nanomedicine, (03 2013): 313. doi:
TOTAL:	**1**	

Number of Papers published in non peer-reviewed journals:

(c) Presentations

Number of Presentations: 0.00

Non Peer-Reviewed Conference Proceeding publications (other than abstracts):

Received	Paper

TOTAL:

Number of Non Peer-Reviewed Conference Proceeding publications (other than abstracts):

Peer-Reviewed Conference Proceeding publications (other than abstracts):

Received	Paper	
08/20/2012	18.00	Zhonghua Xu, Scott Lenaghan, David Gilmore, Lijin Xia, Mingjun Zhang. Automated High Throughput Scalable Green Nanomanufacturing forNaturally Occurring Nanoparticles using English Ivy, Robotics and Automation (ICRA), 2012 IEEE International Conference on. 15-MAY-12, . : ,

TOTAL: **1**

Number of Peer-Reviewed Conference Proceeding publications (other than abstracts):

(d) Manuscripts

Received		Paper
02/24/2013	28.00	Sijia Yi, Leming Sun, Scott C. Lenaghan, Yongzhong Wang, Xinyuan Chong, Zhili Zhang, Mingjun Zhang. One-step Synthesis of Dendritic Gold Nanoflowers with High Surface-Enhanced Raman Scattering (SERS), RSC Advances (02 2013)
02/24/2013	22.00	Sijia Yi, Lijin Xia, Scott C. Lenaghan, Leming Sun, Yujian Huang, Jason N. Burris, C. Neal Stewart, Jr., Mingjun Zhang. Bio-synthesis of Gold Nanoparticles using English ivy (Hedera helix), Journal of Nanoscience and Nanotechnology (11 2012)
02/24/2013	21.00	Scott C. Lenaghan, Yuanyuan Li, Hao Zhang, Jason N. Burris, C. Neal Stewart, Jr., Lynne E. Parker, Mingjun Zhang. Monitoring the Environmental Impact of TiO2 Nanoparticles Using a Plant-based Sensor-network., IEEE TRANSACTIONS ON Nanotechnology (08 2012)
02/25/2013	29.00	Sijia Yi, Yongzhong Wang, Yujian Huang, Lijin Xia, Leming Sun, Scott C. Lenaghan, Mingjun Zhang. Tea Nanoparticles for Immunostimulation and Chemo-drug Delivery in Cancer Treatment, Advaced Functional materials (02 2013)
02/27/2013	20.00	Mingjun Zhang. Fungus-based nanoparticles: Inspiration from Nature for Cancer Therapy, Nanomedicine (01 2013)
05/16/2012	7.00	Leming Sun, Lijin Xia, Sijia Yi, Scott C. Lenaghan, Mingjun Zhang. Biosynthesis of gold and silver nanoparticles using AsparagusLettuce peel, Bioprocess and Biosystem Engineering (05 2012)
05/16/2012	8.00	Lijin Xia, Zhonghua Xu, Leming Sun, Patrick M. Caveney, Mingjun Zhang. Spherical nanoparticles as fillers to tune mechanical properties of silicone matrix, Journal of Nanoparticle Research (04 2012)
05/16/2013	30.00	Scott C. Lenaghan, Jason N. Burris, Karuna Chourey, Yujian Huang, Lijin Xia, Belinda Lady, Ritin Sharma, Chongle Pan, Zorabel LeJeune, Shane Foister, Robert L. Hettich, C. Neal Stewart, Jr., Mingjun Zhang. Biosynthesis and Chemical Analysis of Nanoparticles from English Ivy (Hedera helix L.) , Proceedings of Royal Society of Interface (04 2013)
05/17/2012	10.00	Sijia Yi, Scott C. Lenaghan, Mingjun Zhang, Lijin Xia. Facile synthesis of biocompatible gold nanoparticles with organosilicone-coatedsurface properties, Journal of Nanoparticle Research (05 2012)
06/04/2012	11.00	Lijin Xia, Sijia Yi, Scott C. Lenaghan, Mingjun Zhang. Facile synthesis of biocompatible gold nanoparticles with organosilicone-coated surface properties, Journal of Nanoparticle Research (05 2012)
07/20/2012	13.00	Yongzhong Wang, Leming Sun, Sijia Yi, Yujian Huang, Scott C. Lenaghan, Mingjun Zhang. Naturally Occurring Nanoparticles (NONPs) from Arthrobotrys oligospora as aPotential Immunostimulatory and Antitumor Agent, Nano Letters (07 2012)
08/25/2013	34.00	Leming Sun, Sijia Yi, Yongzhong Wang, Kang Pan, Qixin Zhong, Mingjun Zhang. A Bio-inspired Approach for In Situ Synthesis of Tunable Adhesive, Bioinspiration & Biomimetics (07 2013)

09/09/2010 2.00 Lijin Xia, Scott C. Lenaghan, Mingjun Zhang, Yu Wu, Xiaopeng Zhao, Jason N. Burris and C. Neal Stewart Jr.. Characterization of English ivy (Hedera helix) adhesion force and imaging using atomic force microscopy,
(09 2010)

09/24/2012 19.00 Mingjun Zhang, Jason N. Burris, Karuna Chourey, Scott C. Lenaghan, Yujian Huang, Lijin Xia, Belinda Lady, Ritin Sharma, Chongle Pan, Zorabel LeJeune, Shane Foister, Robert L. Hettich, C. Neal Stewart, Jr.. Identification of the Chemical Nature of Nanoparticles Secreted by English Ivy (Hedera helix), Nature Nanotechnology (submitted) (09 2012)

TOTAL: **14**

Number of Manuscripts:

Books

Received Paper

TOTAL:

Patents Submitted

2012 Jason Burris, Neal Stewart, Scott Lenaghan, David Gilmore, Mingjun Zhang. Biofabrication for nanoparticle production using English ivy (Hedera helix), Provisional Pend.

2010 Mingjun Zhang, Lijin Xia and Scott Lenaghan. Cosmetic compositions including ivy derived nanoparticles, Patent #WO2012047205.

Patents Awarded

2010 Mingjun Zhang, Lijin Xia and Scott Lenaghan. Cosmetic compositions including ivy derived nanoparticles, Patent #WO2012047205.

Awards

2013 Research Fellow Award (Faculty Award of Excellence in Research), College of Engineering, The University of Tennessee, Knoxville.

2012 Featured in the faculty appreciation week by students. One of the two faculty members elected from the College of Engineering for committing excellent teaching and research. The University of Tennessee.

2011 Young Investigator Award (YIP). Office of Naval Research, Department of Defense, USA.

2011 QUETS Scholar of the Week August 29. The University of Tennessee, Knoxville.

2011 Congratulation Letter from US Navy, Chief of Naval Research, Rear Admiral Nevin P. Carr.

2011 Congratulation Letter from Congressman Mr. John J. Duncan for my research work in his district.

2011 Research Fellow Award (Faculty Award of Excellence in Research), College of Engineering, The University of Tennessee, Knoxville.

Graduate Students

NAME	PERCENT_SUPPORTED	Discipline
Laura Yi	0.30	
Yujian Huang	0.30	
FTE Equivalent:	**0.60**	
Total Number:	**2**	

Names of Post Doctorates

NAME	PERCENT_SUPPORTED
Scott Lenaghan	0.80
FTE Equivalent:	**0.80**
Total Number:	**1**

Names of Faculty Supported

NAME	PERCENT_SUPPORTED	National Academy Member
Mingjun Zhang	0.20	
FTE Equivalent:	**0.20**	
Total Number:	**1**	

Names of Under Graduate students supported

NAME	PERCENT_SUPPORTED	Discipline
Andrew Wills	0.10	BME
FTE Equivalent:	**0.10**	
Total Number:	**1**	

Student Metrics

This section only applies to graduating undergraduates supported by this agreement in this reporting period

The number of undergraduates funded by this agreement who graduated during this period: 1.00

The number of undergraduates funded by this agreement who graduated during this period with a degree in science, mathematics, engineering, or technology fields:..... 1.00

The number of undergraduates funded by your agreement who graduated during this period and will continue to pursue a graduate or Ph.D. degree in science, mathematics, engineering, or technology fields:..... 1.00

Number of graduating undergraduates who achieved a 3.5 GPA to 4.0 (4.0 max scale):..... 1.00

Number of graduating undergraduates funded by a DoD funded Center of Excellence grant for Education, Research and Engineering:..... 0.00

The number of undergraduates funded by your agreement who graduated during this period and intend to work for the Department of Defense 0.00

The number of undergraduates funded by your agreement who graduated during this period and will receive scholarships or fellowships for further studies in science, mathematics, engineering or technology fields: 0.00

Names of Personnel receiving masters degrees

NAME
Total Number:

Names of personnel receiving PHDs

NAME
Laura Yi
Total Number: 1

Names of other research staff

NAME	PERCENT_SUPPORTED
Scott Lenaghan	0.20
FTE Equivalent:	**0.20**
Total Number:	**1**

Sub Contractors (DD882)

Inventions (DD882)

Scientific Progress

Please see attachment.

Technology Transfer

Final Technical Report for Project

Mechanics of the Adhesive Properties of Nanoparticles

ARO Grant W911NF-10-1-0114

06/01/2010-05/31/2013

Program Manager

Dr. Stephanie A. McElhinny
Program Manager, Biochemistry, Life Sciences Division
U.S. Army Research Office
Email: stephanie.mcelhinny@us.army.mil. Phone: 919-549-4240

Principle Investigator

Dr. Mingjun Zhang
University of Tennessee, Knoxville
Email: mjzhang@utk.edu. Phone: 865-974-7620

Submitted

November 21, 2013

1. Foreword

We have not only achieved original goals proposed for this research, but also made significant expansion to advance the research subjects related to naturally occurring nanoparticles, and bio-inspired tunable nano-adhesive. Specifically, we have identified mechanical and mechanics roles of the ivy nanoparticles for high strength adhesive, and proteinaceous nature of the ivy nanoparticles, but also expand the effort to understand the complete chemical composition of the ivy nanoparticles, and proposed molecular mechanism of the high strength adhesive. The molecular mechanism of the ivy adhesive could offer totally new view about biological adhesive, and potentially create totally new avenue for bio-inspired adhesive. Currently, there is no plant-inspired adhesive in the market. Ivy adhesive has some truly amazing properties that could highly impact the field of high strength adhesive engineering. We have developed a bio-inspired *in situ* synthesis approach to fabricate a tunable nanoadhesive.

While looking forward to the future, we would appreciate a potential opportunity to continue the work with ARO, and make the research ultimate success for military usage and commercialization. Potential projects include 1) ivy molecular mechanism inspired high strength adhesive, 2) force-activated synthetic biology for novel nanoparticles and nanoadhesive, and 3) AGP-based novel nanomaterials. The team was fortunate to be supervised by Dr. Stephanie McElhinny. We are looking forward to the potential opportunity to continue the work with her.

2. Summary of the most important results

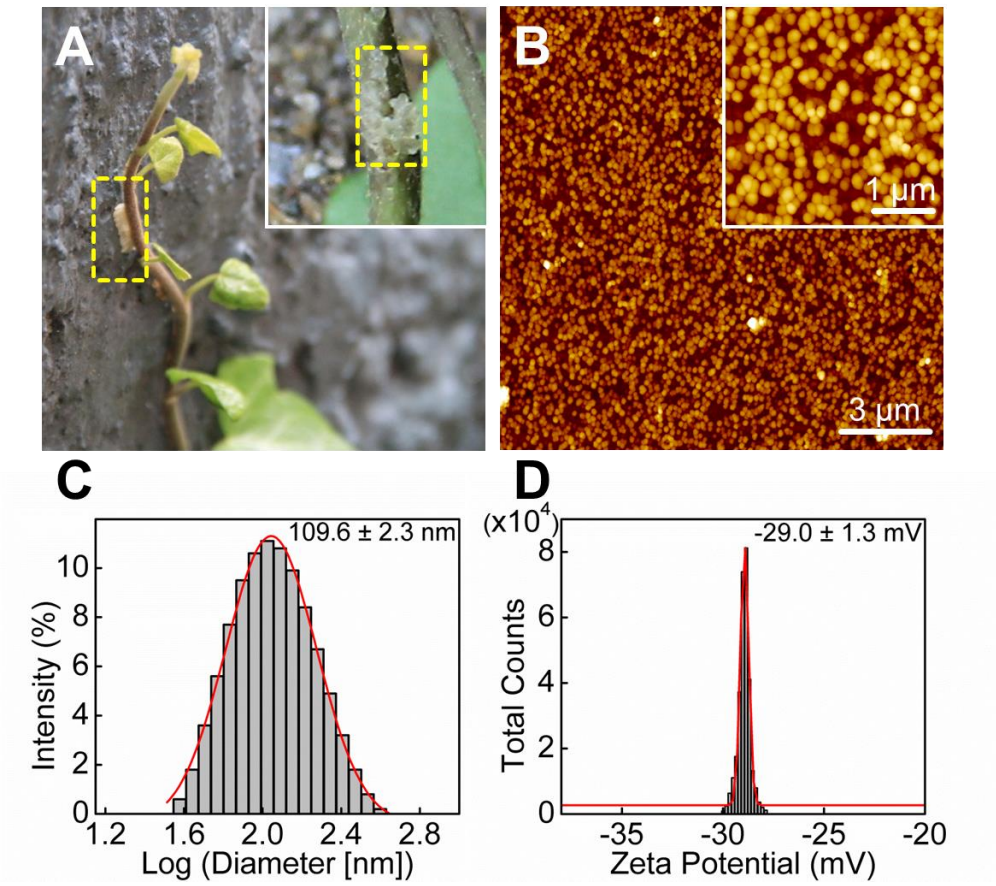

Fig. 1. Characterization of nanoparticles isolated from the adventitious roots of English ivy. (**A**) Ivy shoots attaching to a wall. Abundant adventitious roots can be found in the area enclosed by a yellow rectangle

frame. Inset, adventitious roots formed an adhesive pad at a contact surface (*11, 12*). (**B**) AFM images of purified ivy nanoparticles dispersed on a coverslip. Inset, high magnification view. Scale bars represent 3 μm and 1 μm, respectively. (**C**) Size distribution of the purified ivy nanoparticles in water. Average diameter of the ivy nanoparticles was 109.6 ± 2.3 nm, as measured by dynamic light scattering. (**D**) Zeta potential of the purified ivy nanoparticles in water. The nanoparticles showed a zeta potential of -29.0 ± 1.3 mV at 25 ℃.

As shown in **Fig. 1**, the spherical nanoparticles, abundantly observed in the adhesive secreted from the adventitious roots of English ivy, were hypothesized to contribute directly to the high strength adhesive for surface affixing. Through this research, we have confirmed the hypothesis, and finally determined that the ivy nanoparticles were chemically composed with one type of glycoproteins, abinogalactan protein (AGP), a macromolecule that has been proved to play a similar adhesion function in many plants. This is the first experimental work demonstrating the existence of the *nano-spherical shape AGP*, since the first proposal of a structural model about this proteoglycan/glycoprotein in 1983. Evidence also indicated that the secreted adhesive, containing ivy nanoparticles, adopted the similar principles used by wood adhesive, to strengthen the adherence of rootlets with different substrates. Ivy nanoparticles contribute to the strong adhesion forces by forming an adhesive film at the interface, to increase the mechanical inter-locking between the rootlets and the substrates. The nano-spherical morphology of the ivy nanoparticles enables ivy nanoparticles easy to spread and permeate on the substrates, due to their inherent low viscosity. Driven by the water evaporation, ivy nanoparticles adjusted their shapes to form a film. Pectic polysaccharides and calcium ions were also confirmed to participate in the generation of adhesion forces, by wrapping ivy nanoparticles in a gel-like matrix before hardening.

This discovery of molecular mechanism for this adherence will advance related studies on the crimping phenomenon of other plants, since similar adhesive substance has been observed in many climbing plants. The study on the AGP nanoparticle-mediated adhesion will also inspire us to create high strength industrial glues. The following specific efforts have directly contributed to the discovery of the above molecular mechanism of the high strength ivy adhesive, and prototype engineering of the ivy inspired tunable adhesive.

2.1. Production of ivy nanoparticles

First, a method for the production of ivy nanoparticles and demonstration of the scalability of this process has been developed as shown **Fig. 2**. Briefly, bulk ivy nanoparticles were harvested from cultured adventitious roots through homogenization, filtration and separation through an SEC column. The development of this method was crucial for demonstrating the ability to collect bulk nanoparticles for use in applications, and also to obtain enough nanoparticles for subsequent chemical analysis. A challenge to the collection of ivy nanoparticles was the small size of the root hairs (approx. 10 mm in diameter). Since the root hairs are the only known structures involved in the generation of the nanocomposite adhesive, the first step in the development of a procedure for nanoparticle production was to maximize the production of root hairs, while preventing any external contamination. As a result, a tissue culture method was developed for growing the adventitious roots from cut shoots in sterile Magenta GA-7 (MAG) plant culture boxes. Ivy shoots used for tissue culture were donated by Swan Valley Farms (Bow, Washington) on a weekly basis. Briefly, shoots were cut approximately to 6 inches with one leaf remaining on the top of the shoot. The external surfaces of the shoots were then sterilized and the shoots placed upright into MAG boxes containing nutrient media. The boxes were then sealed and placed into a plant growth chamber with controlled light and temperature. By sealing the MAG boxes, it was possible to achieve 100% humidity in the boxes, which was crucial for maintaining the hydration of the adventitious roots. Using this culture method, it was possible to generate harvestable adventitious roots every two weeks. In addition, adventitious roots grew much denser in the culture system when compared with uncultured plants. Furthermore, the adventitious roots had a much higher concentration of root hairs, owing to the

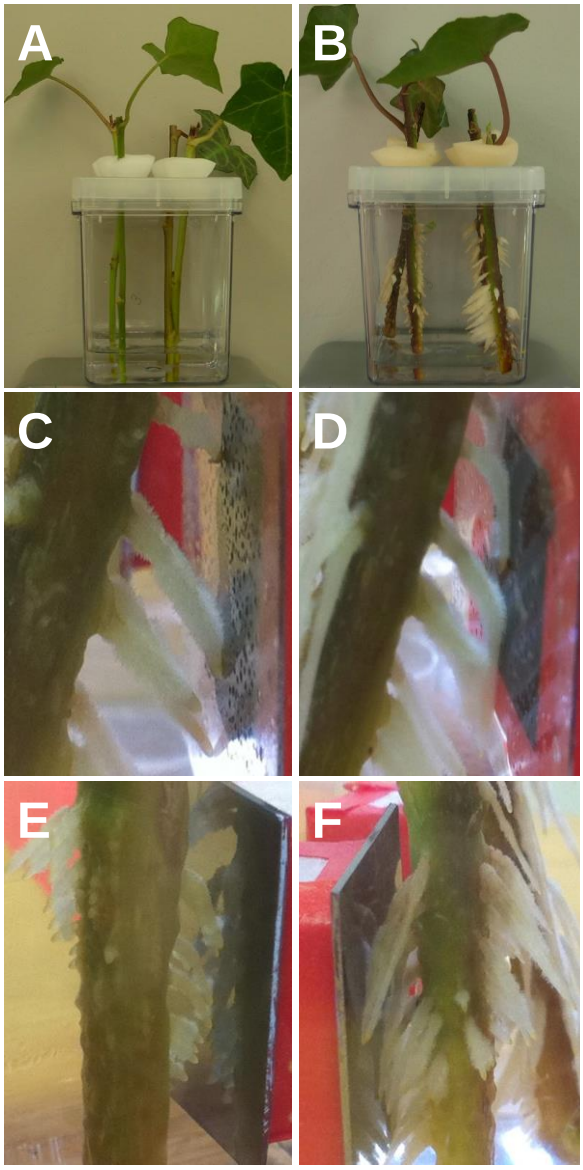

Fig. 2. *In situ* collection of the secretions from the ivy rootlets. (**A**) Ivy rootlets cultivation system. Juvenile shoots were hydrocultured after induction with auxin. (**B**) Adventitious roots appeared after 8~10 days' cultivation. (**C**) A coverslip was vertically fixed, close to the growing tips of the rootlets, in order to facilitate the surface affixing of the adventitious roots to the coverslip. (**D**) The roots grew toward the coverslip in a manner that has been described in details. (**E**) A silicon wafer, instead of coverslip, was vertically fixed to collect the secretions of ivy rootlets. (**F**) Once rootlets showed a tight adherence to the silicon wafer, which usually took 3-4 days, the silicon wafer was removed and the *in situ* collected secretions on the surface was observed with SEM.

high humidity and the increased availability of nutrients. Development of this culture system greatly increased the ability to generate the tissue for nanoparticle secretion, leading to further advances in the design of a robust method for ivy nanoparticle isolation.

With the stable, scalable tissue culture system described above, the next step was to harvest the tissue for isolation of the nanoparticles. Considering the small diameter of the root hairs and the rapid dehydration of the tissue when separated from the adventitious roots, the entire adventitious root was collected for harvesting the nanoparticles. To preserve the integrity of the tissue during the time required for harvesting, the adventitious roots were excised directly into a liquid nitrogen cooled container resulting in an immediate snap freezing of the tissue. After collection of bulk adventitious roots, the roots were stored at -80C. Once an appropriate amount of tissue (more than 1 g) was collected for nanoparticle isolation, the tissue was homogenized at 4C using a mortar and pestle. Manual homogenization was conducted with only a minimum amount of ultrapure water to allow the solution to be easily pipetted out of the mortar. After homogenization, the solution containing a large amount of cell debris, proteins, the polymer adhesive and nanoparticles was obtained. To remove the large debris, the solution was filtered through a 0.2 mm syringe filter and then centrifuged at 1000g to remove any remaining debris. Finally, the sample was dialyzed through a 300 kDa Spectra/Por cellulose ester dialysis membrane overnight at 4C with constant stirring. This high molecular weight (MW) dialysis membrane was effective for removing most proteins, and also salts present in the sample. Smaller MW dialysis membranes were tested; however, the nanoparticles isolated using the 300 kDa membrane represented the purest fraction, and thus this membrane was used for further purification. After dialysis, samples were run on an SECHPLC column for separation of the ivy nanoparticles from the other components.

2.2 Characterization of physicochemical properties of ivy nanoparticles

The stability of the ivy nanoparticles, specifically their UV protective capabilities, to changes in temperature, pH, and prolonged UV exposure were investigated. Results showed that ivy nanoparticles demonstrated relatively strong temperature, pH and UV irradiation tolerance. However, at 100°C, ivy nanoparticles were partially degraded and displayed increased agglomeration, which were modulated by partial protein unfolding. This degradation leads to an increase in the UV extinction spectra of ivy nanoparticles. Considering that 100°C falls well outside of the range necessary for a sunscreen product, the stability analysis from -20°C to 40°C shows that the ivy nanoparticles meet the criteria necessary for stable sunscreen filler. Since high temperatures may still be encountered in the process of manufacturing a sunscreen product incorporating the ivy nanoparticles, such as the sterilization of the ivy nanoparticles using autoclaving, this study had certain guiding significance to the practical operation. Results about the influence of pH variation on ivy nanoparticles showed that the UVA extinction spectra slightly decreased with a decrease of pH values.

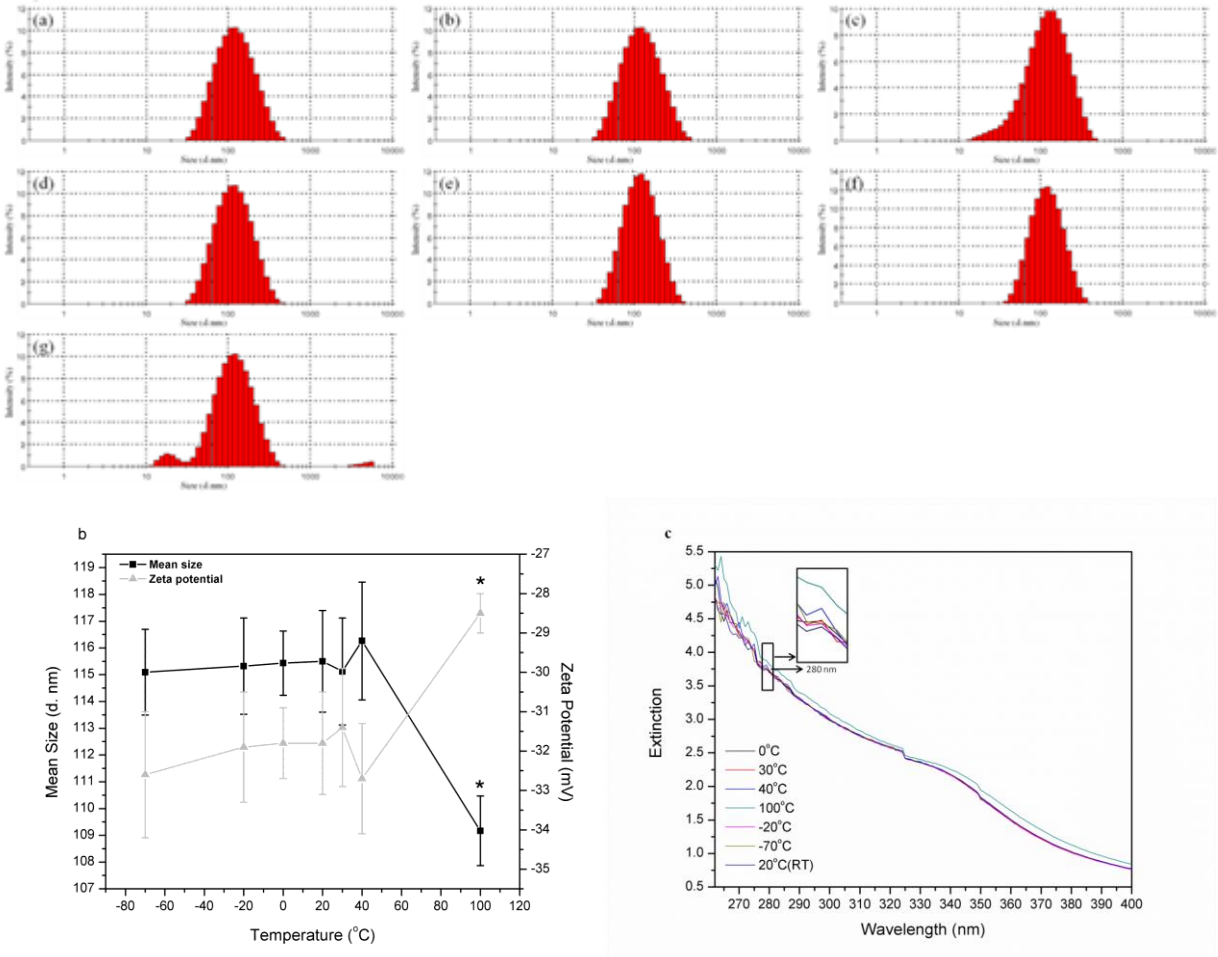

Fig. 3. Temperature influence on ivy nanoparticles. **a.** Size distributions of ivy nanoparticles treated with different temperatures: (a) -70 ℃, (b) -20 ℃, (c) 0 ℃, (d) 20 ℃, (e) 30 ℃, (f) 40 ℃, (g) 100 ℃, **b**. DLS measurements of ivy nanoparticles treated with different temperatures, and **c**. UV extinction spectra of ivy nanoparticles treated with different temperatures.

Nanoparticles were more stable in alkaline solutions than in acidic environments. It was also observed that protein played an important role in modulating three dimensional structures of ivy nanoparticles. The morphology study showed that after removing most proteins from ivy nanoparticles, there were still some

small residues which displayed irregular and asymmetric structures on the surface of mica. Furthermore, the influence of UV irradiation on the ivy nanoparticles was evaluated by UV-Vis spectroscopy and the results indicated that the impact was small and time-independent. In summary, ivy nanoparticles demonstrate the necessary stability to be used as sunscreen filler, with advantages over currently used metal oxide nanoparticles. The increased visual transparency and safety of these nanoparticles make them an attractive candidate to replace metal oxide nanoparticles, leading to less concern over the environmental impact of these nanomaterials.

Previous studies indicated that ivy nanoparticles show increased extinction spectra in the UVA/UVB range and decreased absorbance in the visible region when compared to TiO2 nanoparticles, which endow ivy nanoparticles with a greater UV protective potential and allow them to be transparent to visible light. In the meantime, previous report also mentioned the possibility of investigating the UV extinction property of ivy nanoparticles from a protein perspective. By BCA quantification, the concentration of protein in ivy nanoparticles was around 58%. In this study, factors which may have a possible impact on the morphology and surface reactivity of ivy nanoparticles, especially the influence on protein stabilities, were investigated. The influence of temperature variation on the morphology of ivy nanoparticles and on the UV extinction capability was evaluated by DLS and UV-Vis spectrophotometry. Freshly isolated ivy nanoparticles were treated at 7 different temperatures for 2 hours followed by DLS measurements to obtain the particle size distribution, mean size and zeta potential variations. The mean from three separate trials was compared to determine the standard deviation from experiment to experiment. Results from the measurement show that the mean size of the extracted ivy nanoparticles preserved at room temperature was 115.50 ±1.9 nm (SD stands for the standard deviation of three mean sizes getting from three independent trials, **Fig. 3b**), while 90.3% of the nanoparticles were between 70.90 to 255 nm. The lowest mean size (109.17 ±1.3 nm) was obtained by the ivy nanoparticles treated at 100°C, whereas ivy nanoparticles treated with other temperatures showed little difference in the mean size (**Fig. 3b**). After treating at 100°C for 2 hours, 1.1% of ivy nanoparticles were agglomerated to larger than 4 μm, and 5.2% were in the form of small (11.61~32 nm) nanostructures (**Fig. 3**).

As shown in **Fig. 3**, ivy nanoparticles demonstrated great temperature tolerance over a wide range of variation. Even treated with the extreme temperature for a long time, most ivy nanoparticles still maintained stable nanostructures and steady dispersive state. The temperature-tolerant behavior of ivy nanoparticles was consistent with the physiological characteristics of this plant, which can survive in a wide range of ambient temperatures. Ivy nanoparticles were indicated to participate in the climbing process, in which tolerance over a broad temperature range is an important feature. Zeta potential analysis revealed that the ivy nanoparticles treated at 100°C demonstrated a slightly increased zeta potential compared to other samples, which suggested an increasingly unstable dispersive state of nanoparticles at this temperature. Subsequently, the influence of temperature on the UV extinction spectra was further evaluated by UV-Vis spectrophotometry. 3 ml aqueous solutions of ivy nanoparticles treated at different temperatures were added to quartz cuvettes, and the absorbance was recorded. **Fig. 3c** shows that the ivy nanoparticles demonstrated strong extinction spectra from 260 to 400 nm (UVA/UVB range). However, the UVA/UVB extinction spectra of ivy nanoparticles treated at 100°C displayed a distinct increase compared to other samples.

Compared to the results obtained from DLS, this increased absorbance was attributed to the 5.2% small nano-groups (11.61-32 nm) caused by partial decomposition of the ivy nanoparticles after treating at 100°C. The increased surface-to-volume ratio is believed to enhance the UV absorption of this sample. The structural changes of ivy nanoparticles treated at 100°C were examined by spectrofluorimetry. Intrinsic fluorescence of protein was usually used to observe the denaturation or unfolding of macromolecules.

Fluorescence measurements monitor the state of aromatic side chains within the protein (usually tryptophan due to its strong quantum yield), and intrinsic protein fluorescence can be measured at approximately 350 nm after exciting with 280 nm ultraviolet light while the actual emission wavelength can vary depending on the polarity of the environment.

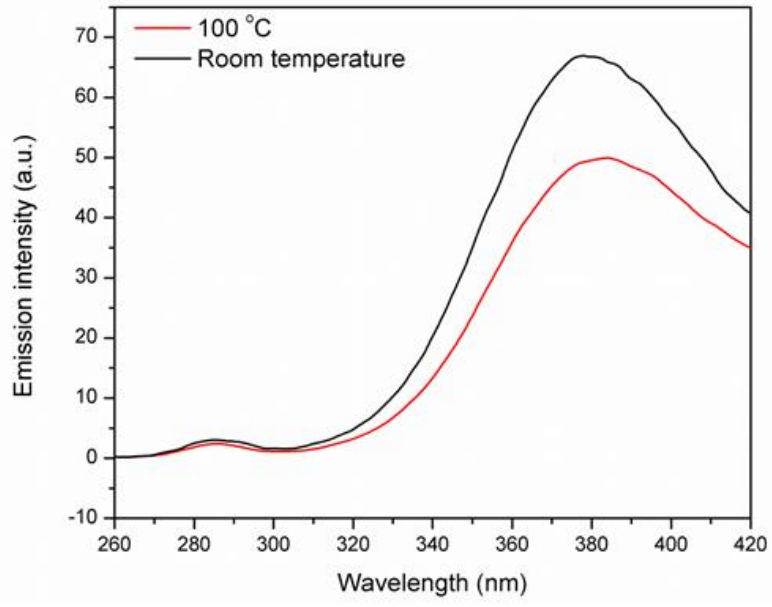

Fig. 4. Intrinsic fluorescence of protein in ivy nanoparticles. Emission spectra of ivy nanoparticles with an excitation of 280 nm. Ivy nanoparticles were treated under room temperature and 100 °C.

Comparing to the folded state, the quantum yield may be either increased or decreased by the unfolding because the fluorescence of the aromatic residues varies in somewhat unpredictable manner in various proteins. Accordingly, an unfolded protein can have either greater or less fluorescence than the folded form. In this study, aqueous solution of ivy nanoparticles treated at 100°C was excited at 280 nm and emission spectra were recorded from 260 to 420 nm.

As shown in **Fig. 4**, ivy nanoparticles preserved at room temperature demonstrated an emission wavelength of around 375 nm. This small drift from the theoretical value (350 nm) was attributed to the interference of other chemical components in ivy nanoparticles. The emission spectra noticeably decreased after treating at 100°C, which indicated the partial denaturation of proteins occurring in ivy nanoparticles. Comparatively, ivy nanoparticles treated with other temperatures didn't show any significant difference in the emission spectra with each other.

Together with results from DLS measurements, it was evident that the degradation and agglomeration process of ivy nanoparticles were accompanied by the partial unfolding process of proteins, which implied that proteins played an important role in maintaining the three-dimensional structures of ivy nanoparticles. Stability of ivy nanoparticles to pH. The sensitivity to pH value was also an important factor when evaluating the application of ivy nanoparticles in sunscreen products. Investigation of the influence of pH variation on the stability and agglomeration of ivy nanoparticles was not only useful for manipulation but also valuable for practical utilizing. In this study, ivy nanoparticles were dispersed in buffers with 7 different pH values followed by DLS measurements and UV-Vis analysis.

Results show that ivy nanoparticles demonstrated diverse mean sizes after dispersing in buffers with different pH values (**Fig. 5b**). The mean size increased from 120.7 ±2.7 to 132.4 ±2.6 nm (SD stands for the standard deviation of three mean sizes getting from three independent trials) accompanying with the decrease of pH values (**Fig. 5b**), which implied that ivy nanoparticles were more stably dispersed in alkaline environments than in acidic ones. Ivy nanoparticles showed more degradation and agglomeration while dispersing in acidic environments (pH 4.0, pH 5.0 and pH 6.0) (**Fig. 5a**). For example, 3.2% of ivy nanoparticles were in very small sizes (17.6~22.5 nm) and 3.9% were agglomerated to larger than 4 μm while dispersing in acetate buffer (0.02 M, pH 4.0) (**Fig. 5a**). These results collectively suggested that ivy nanoparticles were more sensitive to acidic solutions than alkaline ones. As discussed before, protein

played an important role in adjusting three-dimensional structures of ivy nanoparticles, thus should be sensitive to pH variations.

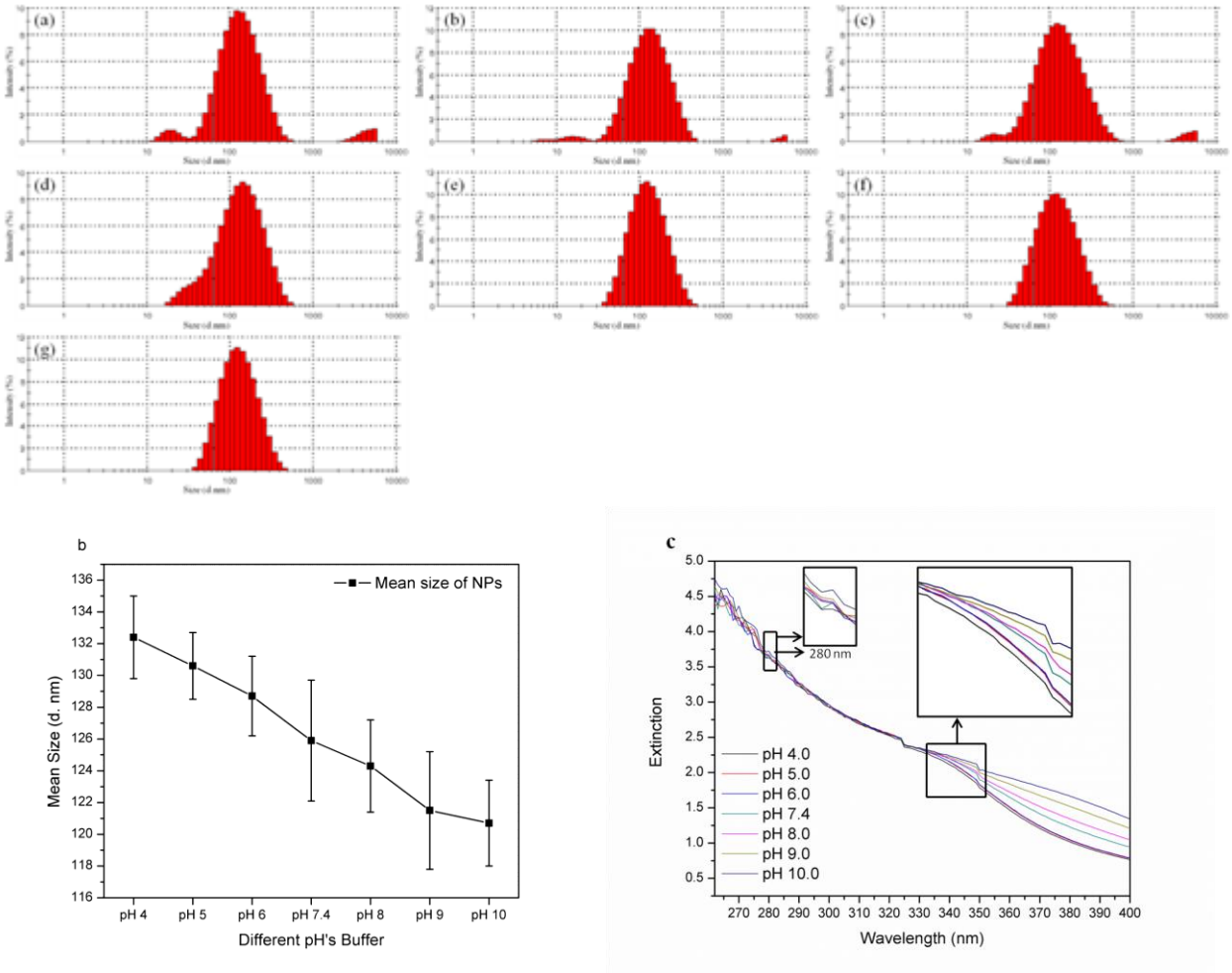

Fig. 5. Influence of pH on ivy nanoparticles. **a.** Size distributions of ivy nanoparticles dispersed in buffers with different pH values: (a) pH 4.0, (b) pH 5.0 (c) pH 6.0, (d) pH 7.4, (e) pH 8.0, (f) pH 9.0, (e) pH 10.0, **b.** DLS measurements of ivy nanoparticles dispersed in buffers with different pH values, and **c.** UV extinction spectra of ivy nanoparticles dispersed in buffers with different pH values.

It was also noticed that the mean size for ivy nanoparticles dispersed in buffers was larger than nanoparticles dispersed in distilled water (**Fig. 5**). This difference was attributed to the interference of salt ions. The UV extinction spectra of ivy nanoparticles dispersed in buffers at different pH's were also recorded using UV-Vis spectrophotometry. As shown in **Fig. 5c**, the UV extinction spectra were measured from 260 to 400 nm. Within the wavelength between 260 and 320 nm (UVB), no distinct spectral difference was observed among different pH values, whereas the UV extinction spectra from 320 to 400 nm (UVA) decreased significantly accompanying with the decrease of pH values. This sub-regional extinction decrease may be attributed to agglomeration of the ivy nanoparticles (**Fig. 5b**). Reduced surface-to-volume ratio may lower the absorption of ultraviolet light.

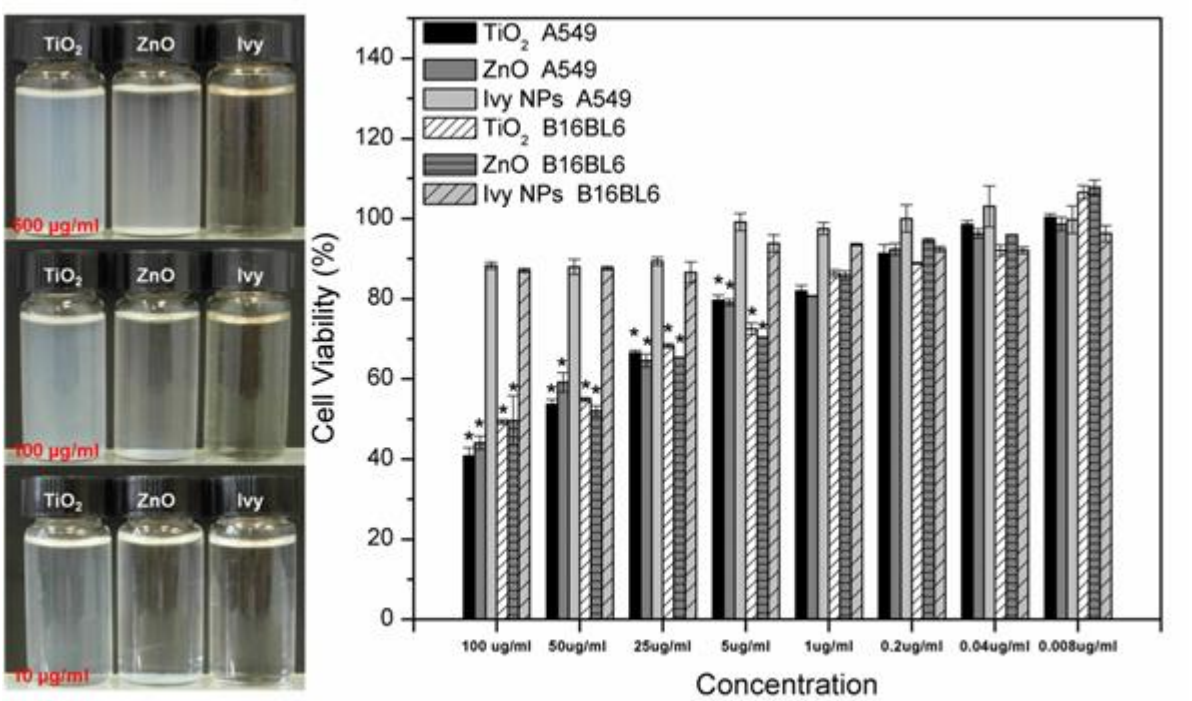

Fig. 6. Visual transparency analysis and cytocompatibility study. **Left:** Three different nanoparticles dispersed in distilled water, and **Right:** MTT assay to compare the cytotoxicity of three different nanoparticles.

Nanoparticles transparency analysis and cytocompatibility Visual transparency is a vital merit for nanoparticles to be used as sunscreen fillers. In this study, the visually transparent property of ivy nanoparticles was compared to TiO2 and ZnO nanoparticles after dispersing in distilled water. Results indicated that ivy nanoparticles presented better transparency in liquid solution (**Fig. 6 Left**). MTT assay was also performed to evaluate the cytotoxicity of three different nanoparticles. Ivy nanoparticles showed lower cytotoxicity to A549 and B16BL6 tumor cells compared to TiO2 and ZnO nanoparticles (**Fig. 6 Right**). For concentrations above 5µg/ml, metal oxide nanoparticles showed distinct cytotoxicity, whereas ivy nanoparticles had little effect. Better cytocompatibility suggested the inherent advantages of naturally occurring nanomaterial.

2.3 Chemical analysis of the ivy nanoparticles

The first step in chemical analysis of the ivy nanoparticles was to confirm that the nanoparticles were organic and did not contain any metals. This is especially important when considering the large number of metallic nanoparticles that can be formed naturally from heavy metal substrates. Numerous studies have demonstrated the potential for plants, including English ivy, to generate nanoparticles from tetrachloroaurate (HAuCl4), silver nitrate (AgNO3), chloroplatinic acid hexahydrate (H2PtCl6 . 6H2O) and iron(III) hloride hexahydrate (FeCl3 . 6H2O). Since the ivy shoots were grown in a cultured environment and were not exposed to variable soil conditions, it was also expected that this would reduce the availability of heavy metal substrates. To rule out the possibility of the ivy nanoparticles containing metallic components, 48.78 mg of ivy nanoparticles were analysed using inductively coupled plasma mass spectrometry (ICP-MS). This technique can be used to detect trace levels of metals in a sample and has recently been expanded to the analysis of metallo-biomolecules, including metallo-proteins. To ensure impartiality, the ivy nanoparticles were analyzed independently by Galbraith Laboratories, Inc. The results indicated that 47 out of 57 elements tested were below the limit of detection of the test at less than

2 parts per million (ppm). These included the most common metals used for the synthesis of nanoparticles from plant extracts, gold, silver, platinum and iron. In addition to the metals that were below the detection limit, only manganese and zinc were found above 30 ppm, and both were still at below trace concentrations (**Fig. 7**). Since no metals were detected above trace levels, it can be concluded that the ivy nanoparticles are, in fact, organic nanoparticles.

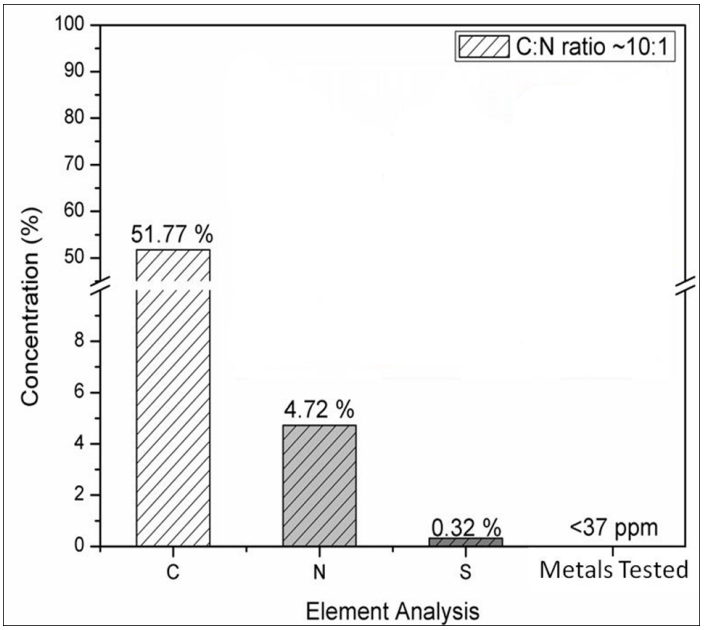

Fig. 7. Diagrammatic representation of the results from the ICP-MS and elemental analysis. As indicated, the C:N ratio was ~10:1, indicating that the nanoparticles were composed of biomolecules. Additionally, ICP-MS revealed that all metals in the ivy nanoparticle fraction were < 37 ppm, confirming that the ivy nanoparticles are organic.

After confirmation of the organic nature of the ivy nanoparticles, the next step was to analyze what type of molecules may be responsible for the formation of the nanoparticles. In previous studies of Boston ivy (Parthenocissus tricuspidata) and Virginia creeper (Parthenocissus quinquefolia), it was found, through immunocytochemical analysis, that the majority of the components in the secreted adhesives were mucilaginous pectins, callose, tanniferous substances and acid mucopolysaccharides. However, nanoparticles were not observed in either of these studies, potentially because of the limitation of the techniques used at the time of these studies. In other biological systems, such as the marine mussel (Mytilus edulis) and polychaete (Phragmatopoma californica), proteins are considered as the main building blocks that lead to the generation of strong adhesive forces. In these two systems, unlike Parthenocissus sp., the adhesives secreted from these organisms have shown the presence of nanoparticles, mainly thought to form from the interactions of negatively charged proteins with divalent cations, forming three-dimensional nanoparticles.

Based on this information, we established a series of experiments to determine the organic components involved in the formation of the ivy nanoparticles. The first experiment conducted was elemental analysis to determine the amount of carbon, nitrogen and sulfur present in the ivy nanoparticles. It was found that the nanoparticles were composed of 51.77% carbon and 4.72% nitrogen (**Fig. 7**). This was a relatively high carbon-to-nitrogen ratio of approximately 10:1 and was indicative of a biomolecule, such as DNA, RNA or protein. In addition, the nanoparticles contained 0.32% sulfur, which again would be expected for a biomolecule, such as a protein, where disulfide bonds play an important role in folding and stability, especially in secreted proteins. While this evidence strongly pointed to the presence of proteins in the nanoparticles, it could not rule out that other biomolecules, such as polysaccharides, may still contribute to the overall structure. In addition, since nanoparticles were isolated, and not an individual chemical component, it was possible that the C:N ratio could have been skewed by the presence of multiple components. As a result, Fourier transform infrared (FTIR) spectroscopy was conducted on lyophilized nanoparticles to obtain further information on the chemical structures of the nanoparticles.

As demonstrated in **Fig. 8**, the FTIR spectrum of the ivy nanoparticles was compared with the spectra generated from a typical protein sample, bovine serum albumin (BSA), and also a popular polysaccharide used in the fabrication of nanomaterials, chitosan. All three samples showed a peak at 1653 cm-1 indicating vibration around C¼O and C–N, along with peaks at 1384–1385 cm-1, indicating C–H bending in aliphatic side groups. Additionally, shared peaks at 2928 cm-1 for both ivy nanoparticles and chitosan, and 2932 cm-1 for BSA, indicate the vibration of C–H present in all samples. When compared with the BSA spectrum, the ivy nanoparticles also shared a peak around 1518 cm-1 for BSA and 1539 cm-1 for ivy.

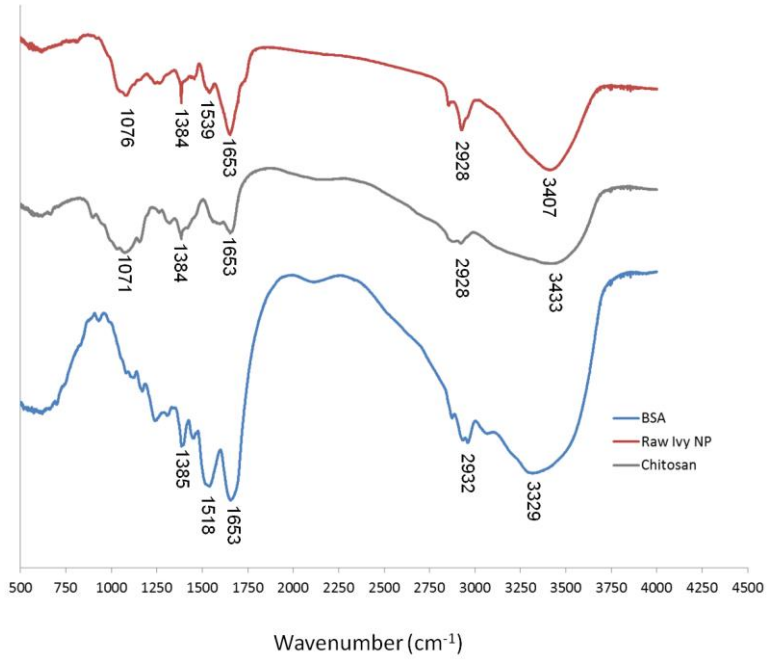

Fig. 8. FTIR spectra of the ivy nanoparticles. The FTIR spectra for the ivy nanoparticles was compared with reference spectra for chitosan (a representative polysaccharide), and BSA (representative proteins). All three samples had a band at 1653 cm^{-1}, indicating vibration around the CO-NH bond, and around 2928-2932 cm^{-1} indicating C-H vibration. In addition, the ivy sample shared a peak at 1071-1076 cm^{-1} with the chitosan sample, indicating vibration of a CO-C bond, typical of sugars. This band was not present in the BSA sample. Similarly, the BSA sample had a strong peak at 1518 cm^{-1}, representing the amide II band, while the ivy nanoparticles had a weak band at 1539 cm^{-1}, indicating a weak amide II band, and the chitosan sample had no peak in this region. The FTIR spectra from top to bottom are: raw ivy nanoparticles, chitosan, and BSA (indicated by color in the online version).

This peak represents the amide II band and is a standard protein peak, indicating the presence of in-plane N–H bending, and the stretching vibrations of C–N and C–C. In standard protein samples, this amide II band often shows similar intensity to the amide I band, as shown for BSA, but the complexity of this band leads to variable intensity and shifts of this peak. In addition to the peak shared by the BSA and ivy nanoparticle sample, the chitosan and ivy nanoparticles shared a peak at 1071 cm-1 for chitosan and 1076 cm-1 for the ivy nanoparticles. This peak was associated with vibration of the CO–C bond typically found in carbohydrates, and thus was not present in the BSA sample. The broad peak present at 3329 cm-1 in the BSA sample indicates the vibration of N–H, and is similar to the broad peaks for chitosan (3433 cm-1) and the ivy nanoparticles (3407 cm-1), where the shift is due to the addition of vibration from O–H. Based on the FTIR data, in combination with the elemental analysis, we believed that the most likely component of the nanoparticles was glycoprotein, owing to the shared amide II band with the BSA spectrum, and the shared CO–C band with the chitosan spectrum. In addition, the shift in the broad peak at 3407 cm-1 indicated that O–H bonds were present, further suggesting the presence of carbohydrate. Based on these data, individual proteins and glycoproteins were believed to form the ivy nanoparticles, and thus we conducted gel electrophoresis to identify individual proteins.

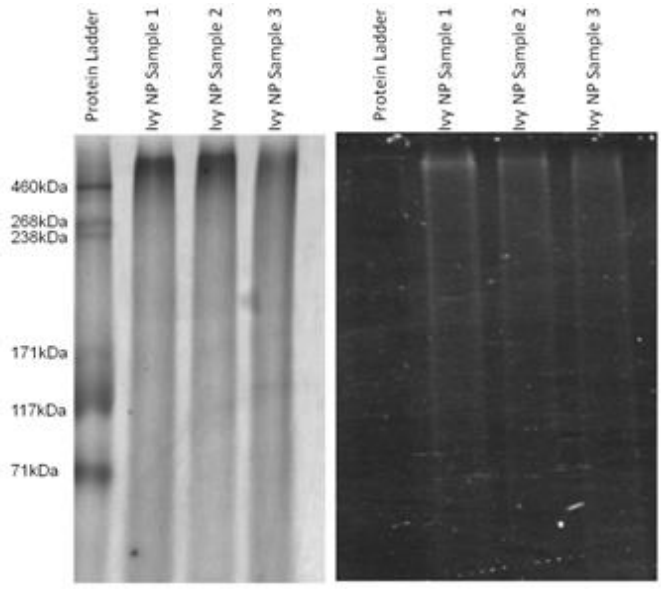

Fig. 9 Results from SDS-PAGE of ivy nanoparticles. Left, results of the silver stain demonstrating the staining of the protein ladder, and all ivy nanoparticle samples. Right, results from glycoprotein stain showing positive staining for the high molecular weight nanoparticle band. Samples 1, 2, and 3 represent nanoparticles isolated from three separate trials. Note the lack of staining of the non-glycosylated proteins from the standard ladder.

Several different gel electrophoresis techniques were evaluated in this study to determine whether the proteins and glycoproteins could be separated from the ivy nanoparticles. It was determined that sodium dodecylsulfate polyacrylamide gel electrophoresis (SDS-PAGE) with a 5% stacking gel and 10% resolving gel yielded the best results for the ivy nanoparticles. In addition, the samples were pre-treated with 2 M thiourea, 8 M urea and 3% SDS, to completely solubilize the nanoparticles, which reduced the background staining. After electrophoresis for 4 h at 180 V, duplicate gels were stained with either the Pro-Q Emerald 300 Glycoprotein Stain Kit (Molecular Probes, Inc., Eugene, OR) or the PlusOne Silver Staining Kit (APBiotech). For reproducibility, ivy nanoparticles isolated from three different isolation procedures by two different researchers were tested. Surprisingly, only one high MW band (greater than 460 kDa) was observed in all of the ivy nanoparticle samples, despite the harsh denaturing conditions used (**Fig. 9**). This high MW band stained positive for protein, using the silver stain, and glycoprotein, using the Pro-Q glycoprotein stain (**Fig. 9**). When comparing the two stains, it was observed that the glycoprotein stain did not cross-react with the non-glycosylated proteins present in the protein ladder (**Fig. 9**). To ensure that the presence of the glycoprotein band was always associated with the ivy nanoparticles, three separate isolations were conducted using different batches of adventitious roots. As shown in **Fig. 9**, the band was consistent across all three samples. This confirmed that the ivy nanoparticles were composed of at least one, if not several glycoproteins. Owing to the high MW of the band, and the potential for the ivy nanoparticles to have survived the denaturing conditions, the possibility still exists that the ivy nanoparticles are composed of multiple proteins and glycoproteins. Further studies are necessary to determine the three-dimensional crystal structure of the ivy nanoparticles and to identify whether multiple copies of a single protein or multiple proteins combine to form the ivy nanoparticles.

In order to test the hypothesis that the ivy nanoparticles secreted by the root hairs of English ivy are composed of AGPs, the purified nanoparticles were characterized by SDS-PAGE and Western blotting. The AGPs can be detected by Yariv phenylglycoside dye, also called β-glucosyl Yariv (β-GlcY) reagent, which selectively binds to the AGPs through recognizing both given protein moieties and β-1, 3-galactan side chains with more than five residues. Ivy nanoparticles purified by SEC or by dialysis were detected both with Coomassie brilliant blue and with 0.2% (w/v) β-GlcY dye, demonstrating characteristic AGP-like smear bands with a high molecular weight. This result was further confirmed by Western blotting analysis. The ivy nanoparticles purified by two methods were identified with monoclonal antibodies, JIM 13 and JIM 14, which can selectively recognize the glycan epitopes of AGPs.

2.4 Role of the ivy nanoparticles in generating high-strength adhesion

AGP is one of the most complex glycoprotein/proteoglycan families found in the extracellular matrix (ECM) of plants. The diversity of the protein backbone and the complexity of the anchored glycans confer the macromolecule with multiple physiological functions in the growth of plants, such as signaling, cell wall plasticizer, guiding pollen tube growth, and many others. The AGPs on the stigma surface were believed to act as an adhesive base for pollens, indicating the adhesion function that AGPs play in plants. Moreover, gum arabic, a commercial product of AGPs extracted from the acacia tree has been widely applied as an adhesive in the stamp industry.

The AGPs secreted from the adventitious roots of English ivy likely play a similar adhesion function as those observed on the surface of stigma. Like other types of AGPs, ivy nanoparticles showed an extremely low viscosity in solution. For all glues, an adhesive must initially wet the surface, a spreading behavior which is crucial for their performance. In general, the lower the viscosity is, the better wetting effect can be achieved by the adhesive liquid. Nano-spherical AGPs show advantages of permeating into the tiny gaps on the rough surfaces of substrates, leading to a well spreading of adhesive on the surfaces and an intimate contact with the substrates. After the wetting process, the adhesive on the substrates will then harden to form a solid in order to achieve an adhesion function. This hardening process is usually caused by water evaporation. A similar drying process of plant adhesive was observed on the adventitious roots of English ivy and the climbing organs of other plants. Charles Darwin made an accurate description of this phenomenon by stating that "the rootlets first secrete a slightly viscid fluid, and that they subsequently absorb the watery parts, and ultimately leave a cement".

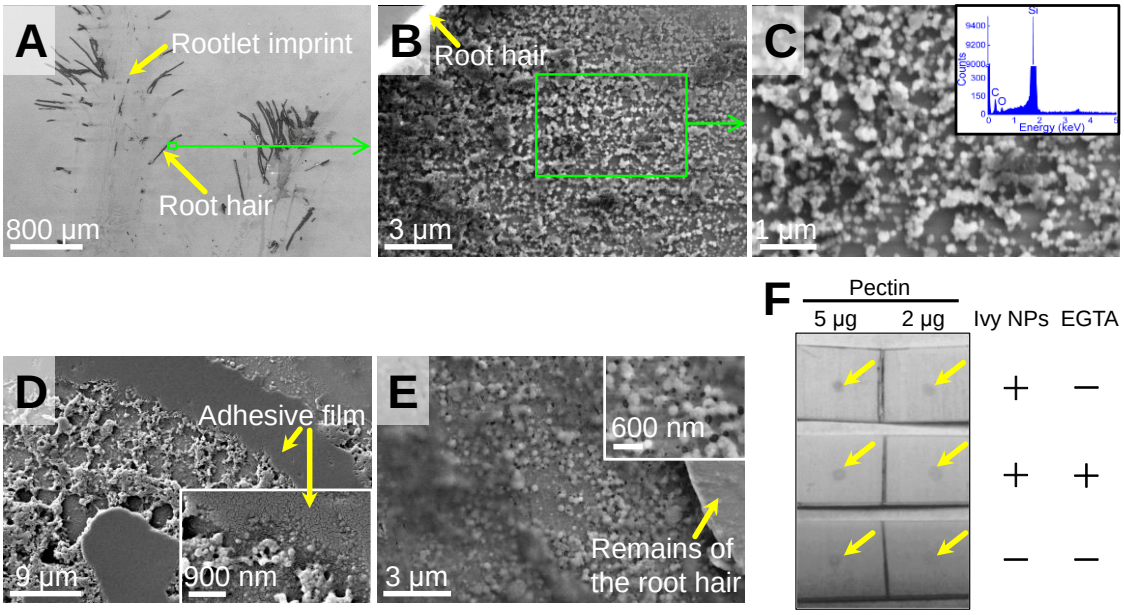

Fig. 10. *In situ* observation of the ivy adhesive and dot blotting analysis of the interactions between pectin and ivy nanoparticles. (**A**) Scanning electron microscope (SEM) image of the rootlet imprints on a silicon wafer. Contour of the adventitious roots and the remains of the root hairs are visible. The scale bar is 800 µm. (**B**) Enlarged SEM image of the area in the green frame of (A). Abundant nano-spherical particles were observed on the surface. Nanoparticles demonstrated a strong tendency to agglomerate and to form large pads. The scale bar is 3 µm. (**C**) Enlarged SEM image of the area in the green frame of (B). The scale bar is 1 µm. Inset, energy-dispersive X-ray (EDX) spectra of the secretions on the silicon wafer. Except for Si, C and O were the main chemical elements of the nanostructures. (**D**) SEM image of the film formed by ivy adhesive. Inset, high magnification view of the film. The scale bars are 9 µm and 900 nm, respectively. (**E**) SEM images of the secreted adhesive underneath the root hairs. Nanoparticles were wrapped in a gel-like porous matrix. Inset, high magnification view of the scaffold. The scale bars are 3 µm and 600 nm, respectively. (**F**) Interactions between pectin and ivy nanoparticles were studied by dot blotting. 5 µg and 2 µg of dissolved pectin extracted from citrus fruit were dotted on the PVDF

membranes. After blocking, PVDF membranes were then incubated with 5 mg/ml ivy nanoparticles dispersed in Tris-buffered saline (TBS, pH 7.6). 10 mM EGTA and 2 mM $CaCl_2$ was selectively added into the incubation, to study the role of calcium ions in this interaction. Membranes were then incubated with antibodies as the procedure for Western blotting. Stronger dot signal suggested that more ivy nanoparticles were retained by the pectin. Results determined the Ca^{2+}-mediated interactions between ivy nanoparticles and pectin, while EGTA blocked this interaction by chelating Ca^{2+} ions.

The secretion and drying processes were reflected on the silicon wafers. Highly abundant ivy nanoparticles were found, surrounding the rootlet imprints, with an average size close to the purified nanoparticles (**Fig. 10A, 10B and 10C**). Besides, the secreted nanoparticles displayed a high tendency to aggregate, and to form large chucks of pads (**Fig. 10B**). The aggregation property of AGPs has been reported before. Apparently, the agglomeration of ivy nanoparticles and the resultant formation of large pads suggested a trend to form a film between the rootlets and the substrates (**Fig. 10D**). This adhesive film is likely the "cement" mentioned by Charles Darwin.

2.5 Principles Extracted from High Strength Adhesive Secreted by English Ivy

2.5.1 Tunable Synthesis Induces Tunable Adhesive Properties

As an effort towards engineering applications, we also investigated nanoparticles, nanofibers, and nanoclays for their filler effects on tuning Young's modulus of silicone matrix, a material with broad in vivo applications. Nano-fillers with different shapes, sizes, and surface properties were added into silicone matrix, and then their filler effects were evaluated through experimental studies. It was found that spherical nanoparticles could clearly improve Young's modulus of the silicone matrix, while nanoclays and carbon nanofibers had limited effects. Smaller spherical nanoparticles were better in performance compared to larger nanoparticles. In addition, enhanced distribution of the nanoparticles in the matrix has been observed to improve the filler effect. In order to minimize toxicity of the nanoparticles for in vivo applications, spherical nanoparticles coated with amine, acid, or hydroxide groups were also investigated, but they were found only to diminish the filler effect of nanoparticles. This result demonstrated that spherical nanoparticles could serve as fillers to tune Young's modulus of silicone matrix for potential applications in medicine. Finally, we have developed multiple methods for the synthesis of AuNPs using English ivy as the substrate. In the first method, we have used actively growing English ivy shoots to develop a sustainable system for the production of ivy nanoparticles. The second method was developed using the extract from the adventitious roots of English ivy. The nanoparticles formed using both methods were compared to determine the size distribution, morphology, and chemical structure of the nanoparticles.

Apart from the nanocomposite structure observed from English ivy adhesive, we also investigated the biological system of the adhesive synthetic process which was used as a model for bio-inspired adhesive design. First, tunable adhesive properties were achieved by tuning biosynthetic process. In nature, English ivy needs tunable adhesive strength to climb different surfaces, for instance, substrates with different surface properties, or humidity in various environments. Specifically, the adhesive property was tuned by biological synthetic process which can control the amount of the synthesized adhesives, concentration of the ivy nanoparticles and various contents of the adhesives. Therefore, this mechanism introduces tunable synthetic processes to achieve tunable properties of bio-inspired adhesive.

A principle extracted from the biological process of English ivy adhesive secretion is the in situ biosynthetic process of the ivy nanoparticles. The ivy nanoparticles and nanocomposite adhesives were all assembled in the same biological system, which provides distinct advantages compared to other nanocomposite synthetic processes, such as solution casting and melt blending. It has been demonstrated in the literature that uniform distribution of nanoparticles in adhesive matrix usually is necessary to

achieve enhanced properties of the nanocomposite. On the contrary, in absence of repulsive interactions, van der Waals attraction between nanoparticles favors clustering and aggregation, and therefore induces defects in nanocomposite materials. The in situ biosynthetic process from English ivy not only provides uniform distribution of the nanoparticles, but also improves the interactions between nanoparticles and matrix. The in situ biosynthesis of nanoparticles from English ivy was believed to contribute to the high strength of the English ivy adhesive through improving the nanoparticle's distribution and the interactions between nanoparticles and the adhesive matrix.

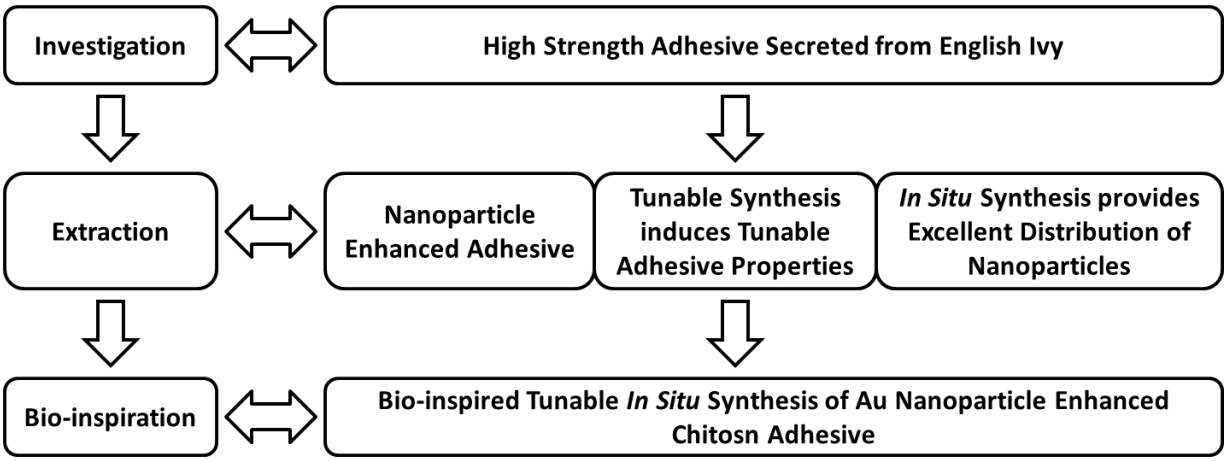

Fig. 11. Schematic of the bio-inspired approach

Inspired by the English ivy adhesive (**Fig. 11**), we hypothesize that the adhesive property of a nanocomposite adhesive may be improved by tuning nanoparticle synthesis process in situ for optimal concentration, distribution and shape anisotropy in the adhesive matrix. To validate this hypothesis, we set up a simple experimental system by in situ tuning the growth of Au nanoparticles in chitosan, which was used as a matrix and a reducing agent. A summary of chemical concentrations for different types of samples were illustrated in Table 1, which was used to further verify the tunable properties.

To determine the adhesive properties of the bio-inspired adhesive fabricated through in situ synthesis of Au nanoparticles in a Chitosan (CS) matrix, a lap shear test was used to measure the adhesion strength of all the samples. The adhesion strength of the pure CS was ~260 KPa for all reaction times, which did not show significant changes (**Fig. 11**). However, there were significant increases in the adhesion strengths for all CS nanocomposites (CSNC), i.e., 0.1, 0.5 and 1 Au CSNC for all reaction times. The 0.1 and 1 Au CSNC showed the max adhesion strength after 24h (527 KPa) and 6h (518 KPa) reactions, respectively, which increased around 100 % compared to the pure CS. Interestingly, the 0.5 Au CSNC had the max adhesion strength of 927 KPa (2.5 fold higher than the pure CS) after 3d reaction. Compared to 0.1and 1 Au CSNC, the 0.5 Au CSNC showed a significantly higher adhesion strength for 1-7d reaction times, indicating that the adhesive property of the bio-inspired adhesives were tuned by the concentration of in situ synthesized Au nanoparticles in the CS matrix.

It is well known that the addition of nanoparticles will lead increase of adhesive properties for different polymer matrix. The adhesive prosperity of the nanocomposite adhesive is often related to a change of the failure mode of the adherends. The failure for adherends bonded with the pure polymer may occur at the interface (i.e., adhesive failure), while for the adherends bonded with nanoadhesive containing proper nanoparticle concentration, the failure cohesive was found to be a dominant mode. However, if continued increase in the nanoparticles concentration, the failure mode of the adherends could change to be interfacial again. Therefore, an optimized concentration of the nanoparticles in the polymer

nanocomposite is a critical parameter to achieve maximal adhesive properties. In this study, the failure mode of the 0.1 Au CSNC from beginning to max adhesive strength (from 6h to 24h reaction time) could be present at the interface, while the failure mode for the adherends changed to the cohesive zone after 24h. For the 0.5 Au CSNC, the failure mode was still present at the cohesive zone until the adhesive strength reached max value at 3d reaction time. The increase in the adhesive strength before the max value could be due to the increase in the cohesive forces by the Au nanoparticles. After reaching the max adhesion strength, the failure mode changed back to be interfacial again due to the exceeding concentrations of Au nanoparticles in the CS matrix. Apparently, the failure mode of the 1 Au CSNC was interfacial for all reaction times, which led to the continuous decrease in the adhesion strength from beginning to the end of the reaction.

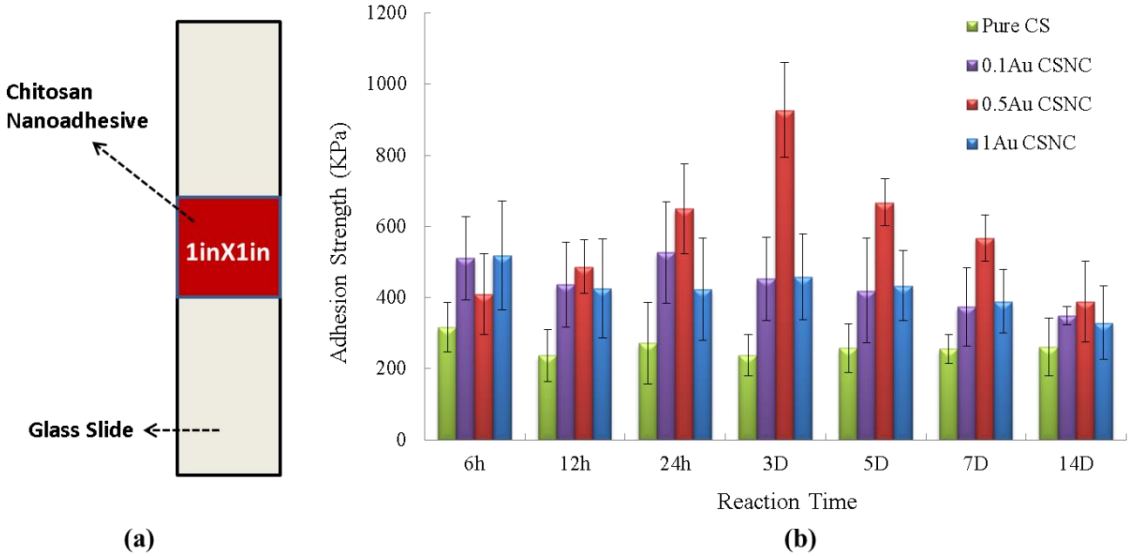

Fig. 12. Schematic of the lap shear test set up (a), and resulted adhesion strength for different samples after different reaction times (b).

A uniform distribution of nanoparticles in the matrix usually is necessary for the full usage of the nanoparticles property to achieve optimal performance of the nanocomposite. However, in the absence of repulsive interactions, van der Waals attraction between nanoparticles favors clustering and aggregation. Thus, nanoparticles tend to macrophase separate and aggregate in the host matrix. Nanoparticles can be prevented from aggregating by sonication and surface modification.

Traditionally, surfactants, coupling agents, and polymer brushes have been widely used to stabilize the nanoparticles. In this study, simple in situ synthetic process without any treatments was applied to achieve excellent nanoparticle distribution in the bio-inspired adhesive. The distributions of the Au nanoparticles in the nanoadhesive were observed by SEM at the fracture surfaces of the samples after adhesion tests. **Fig. 13a-c** showed the distributions of 0.1 Au CSNC after 1d, 3d, and 14d reactions, **Fig. 13d-f** and **Fig. 13g-i** revealed the distributions of 0.5 and 1 Au CSNC after 1d, 3d, and 14d reactions separately. It's obvious that all of the samples have good distributions due to the in situ synthetic process, except the 0.5 Au CSNC after 14d reactions (**Fig. 13f**).

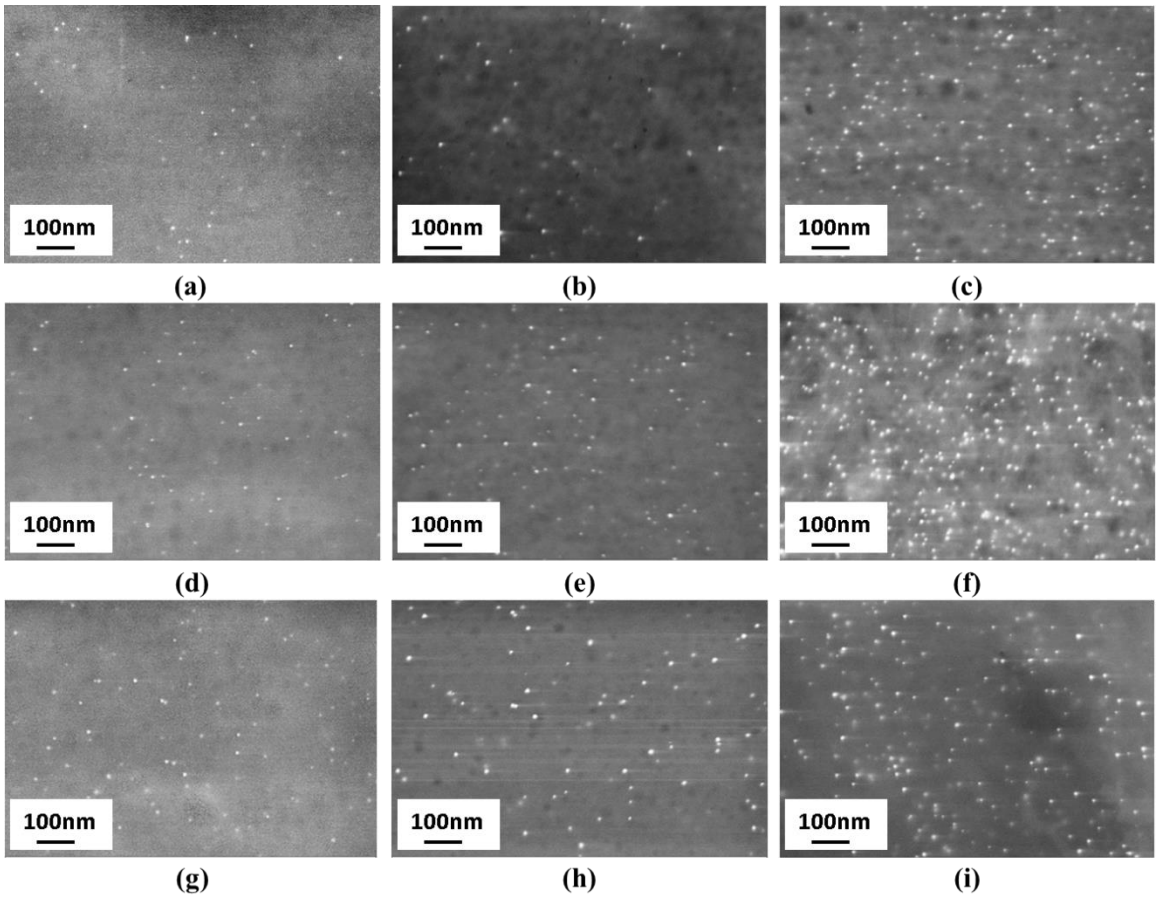

Fig. 13. SEM images of Au nanoparticle's distribution in the bio-inspired nanoadhesive of 0.1 Au CSNC after 1 day (a), 3 days (b) and 14 days (c) reactions, 0.5 Au CSNC after 1 day (d), 3 days e) and 14 days (f) reactions, 1 Au CSNC after 1 day (g), 3 days (h) and 14 days (i) reactions.

Unconspicuous aggregation was observed in this sample, which was due to the overload of the anisotropic Au nanoparticles in the CS. This result demonstrated the in situ synthetic process provides good distribution of Au nanoparticles in the bio-inspired adhesive.

Real-time in situ synthesis of the Au nanoparticles in CS matrix was monitored by the UV-Vis spectroscopy. The UV-Vis spectrum has been used to elucidate the effects of the concentrations, shapes and aggregations of the nanoparticles on the adhesive properties of the bio-inspired nanoadhesive. UV-Vis spectroscopy is an important technique to evaluate the formation and stability of the metal nanoparticles. The well-dispersed spherical Au nanoparticles in solution usually show a sharp surface Plasmon resonance around 510 to 530 nm in the spectrum. As shown in **Fig. 14**, all of the samples had this characteristic peak except for the pure CS, which means that the spherical Au nanoparticles formed in the CS matrices in 0.1, 0.5 and 1 Au CSNC samples. However, differences among the spectra of the three samples were mainly found in the broad plasmon bands in the longer wavelength region, which extends well into the near infrared region in some adhesive solutions. As shown in **Fig. 14a-c**, the 0.1Au CSNC showed gradual increased absorbance in the longer wavelength region for 6-24h reaction times, and 0.5 Au CSNC also had similar increases in UV-Vis absorbance from beginning of the reaction to 3d reaction time, whereas the 1.0 Au CSNC didn't show any increase for all reaction times. This long wavelength absorption indicated significant anisotropy in the shape of the Au nanoparticles, which was well supported by the morphology results of the SEM images (**Fig. 15**).

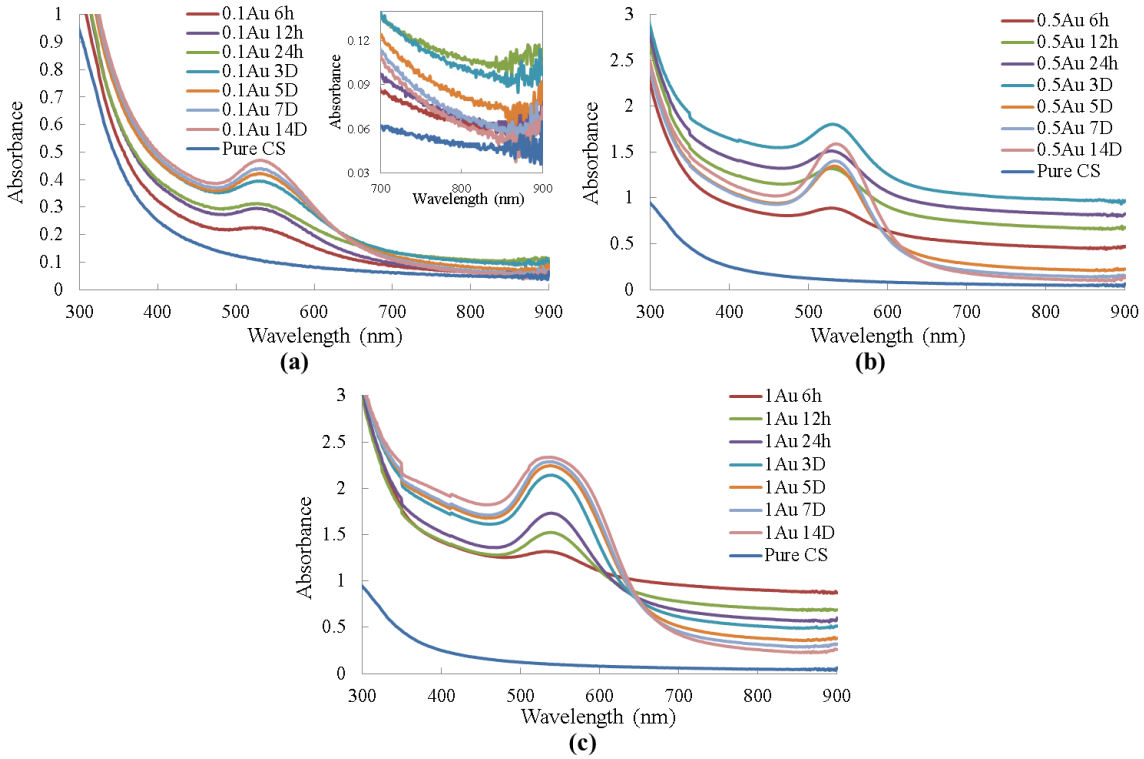

Fig. 14. UV-Vis absorption spectra of the in situ synthesized Au nanoparticles in 0.1 Au CSNC (a), 0.5 Au CSNC (b), and 1 Au CSNC (c) after different reaction times.

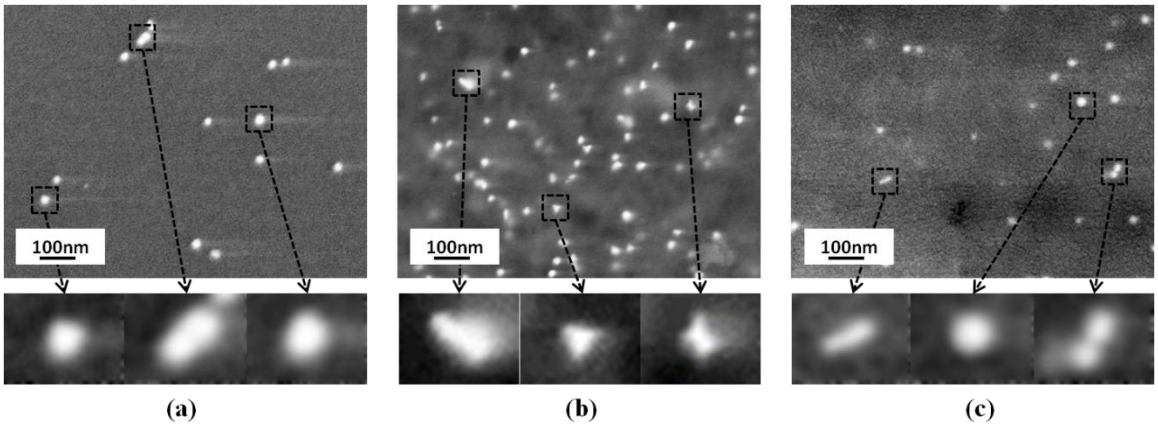

Fig. 15. SEM images of anisotropic Au nanoparticles in the bio-inspired nanoadhesive with triangular and cylindrical shapes.

The interaction energies between nanoparticles and the adhesive matrix are determined by the ratios of their surface area to volume, whereas the ratio is related to their shapes. The interactions between spherical nanoparticles and the matrix are the smallest, due to their smallest surface area to volume ratio. For the 0.1 and 1 Au CSNC, the concentrations of spherical Au nanoparticles increased from the beginning to the end of the reactions, but the changes of concentrations of their anisotropic nanoparticles were different. The 0.1 Au CSNC had the highest concentration of anisotropic nanoparticles after 24h reaction, which supports the maximal adhesion strength at the same time point.

However, concentrations of the anisotropic nanoparticles of the 1 Au CSNC decreased from the beginning to the end of the reactions, which was consistent with the decreasing trend of the adhesion

strength for all reaction times. The UV-Vis spectra of the 0.5 Au CSNC was completely different from both 0.1 and 1 Au CSNC.

The concentrations of the spherical and anisotropic nanoparticles gradually increased to max values after 3d reactions. Interestingly, there was a dramatically decrease in the concentrations of both spherical and anisotropic nanoparticles after the max values, presumably due to aggregation of the nanoparticles in the adhesive solutions. This decrease also well supported the decrease trend in the adhesion strength from the lap shear test.

It has been demonstrated that the addition of nanoparticles to polymer adhesives increased the adhesion strength only when the nanoparticles interacted with the polymer matrix. For example, the incorporation of hydroxyl-treated nanoclays into polyurethane adhesives improved the shear strength by 170%. On condition that the nanoparticles do not react with the polymer adhesives, they may still increase the mechanical properties of the nanocomposite, but do not increase adhesion strength. For better understanding of the interactions between Au nanoparticles and CS, FTIR analysis was applied to the bio-inspired nanoadhesive. The infrared measurements reveal few differences among the spectra of the pure CS, 0.1, 0.5, and 1 Au CSNC (**Fig. 16**). However, due to the inclusion of the Au nanoparticles in the CS matrix47, a clear shift of the amide II + NH2 bending mode was observed for the three bio-inspired samples. The spectral shift probably resulted from an interaction between the amine groups of CS and the Au nanoparticles. Although the three samples of the bio-inspired nanoadhesive showed shifts, the 0.5 Au CSNC had the biggest shift from 1560 to 1577 cm-1, which supports the highest adhesion strength for this sample. These results demonstrate that due to the larger ratio of surface to volume, the interactions between anisotropic nanoparticles and CS were stronger than that between spherical nanoparticles and CS. Therefore, the anisotropy of the Au nanoparticles plays an important role in the adhesive properties of the bio-inspired nanoadhesive by affecting the interactions between nanoparticles and CS.

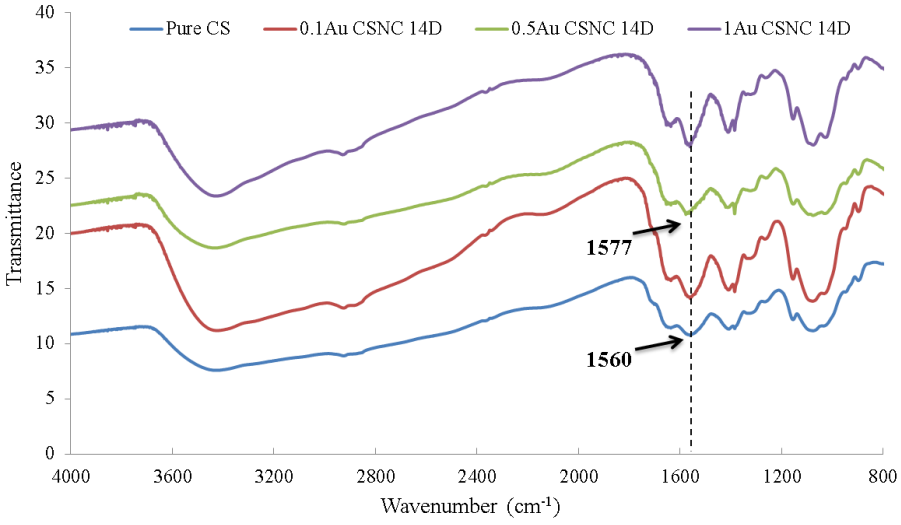

Fig. 16. FTIR results of the bio-inspired nanoadhesive

The viscosity as a function of shear rate and reaction times for the pure CS, 0.1, 0.5, and 1 Au CSNC were further characterized. As shown in **Fig. 17**, for all bio-inspired adhesive samples, the observed viscosity appears to be consistent with the adhesion strength.

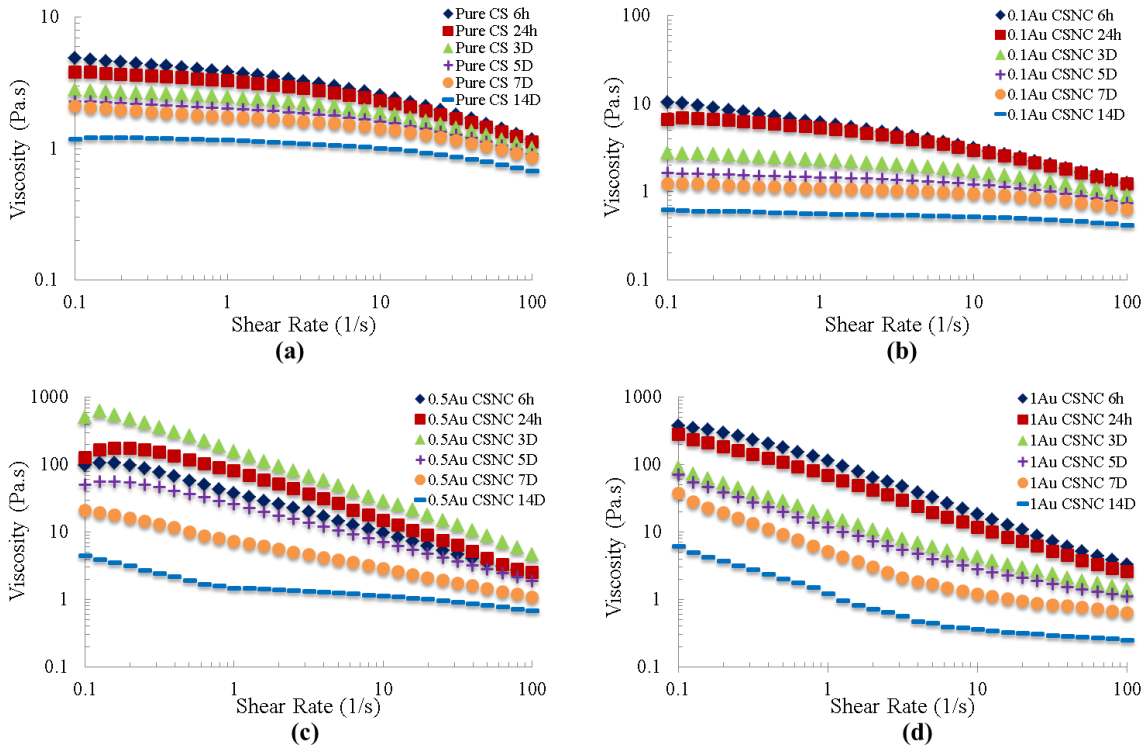

Fig. 17. Viscosity of pure CS (a), 0.1 Au CSNC (b), 0.5 Au CSNC (c) and 1 Au CSNC (d).

Due to the chain swelling of the CS decreasing the entanglements, the viscosities of pure CS slightly decreased with increasing of the reaction time (**Fig. 17**). For the 0.1 Au CSNC, the viscosities (Figure 16b) increased slightly compared to the pure CS. Newtonian behaviors, i.e., no viscosity variation with the changing of the shear rate, were observed in pure CS and the 0.1 Au CSNC with the shear rate lower than 10 1/s; however, due to the entanglements of the molecular chains in the CS, pseudoplastic behaviors (also called shear thinning), i.e., the viscosities decreasing with increasing of the shear rate, were observed at the shear rate higher than 10 1/s. The pseudoplastic behaviors were seen from the 0.5 and 1 Au CSNC for all the reaction times. This behavior presumably resulted from higher concentrations nanoparticles occurred in samples that increase the solution inertia and make the polymer chains easier to be aligned.

However, the viscosities for all three Au CSNC were drastically improved compared to the pure CS (**Fig. 17b-d**), which were consistent with the changing trend of the adhesive properties. Max viscosity was observed after 3d reactions for the 0.5 Au CSNC, which was higher than all the other samples. Even though the viscosities of the 1 Au CSNC continuously decreased from the beginning to the end of the reactions, they are all higher than pure CS.

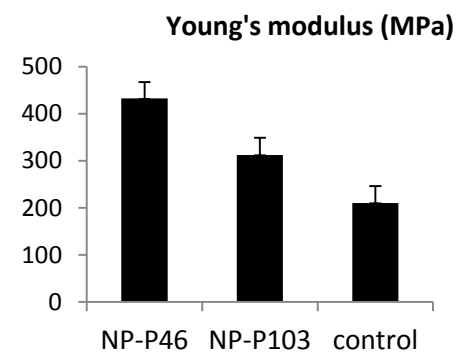

Fig. 18. Moduli of silicone matrix with two different sizes of polystyrene nanoparticles as fillers. Smaller polystyrene nanoparticles had a better performance in enhancing Young's moduli of the composites.

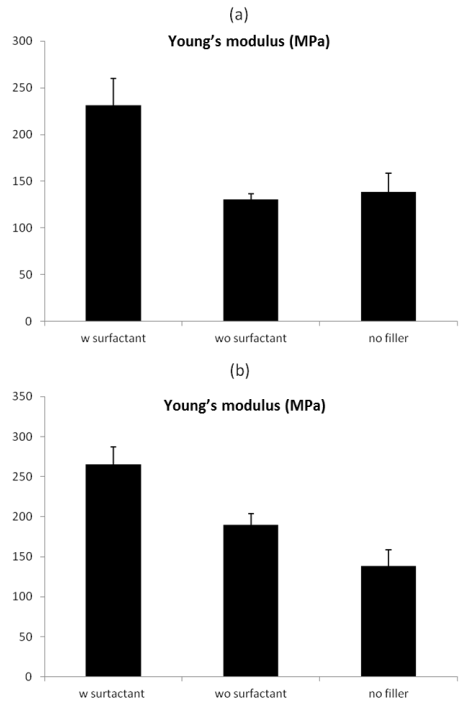

Fig. 19 Surfactant enhanced nanoparticle distribution and the mechanical performance of nanoparticles as filler for TiO_2 (a) and ZnO (b) nanoparticles.

Both experiments and simulation studies have demonstrated that the shape of the nanoparticles is very important for the viscosity properties, and only the spherical nanoparticles have shown the decreased viscosity. The uniqueness of the spherical nanoparticles could be the reason of the fewest amounts of the nanoparticles involved in the interactions due to their compact geometry. It is remarkable that the 0.5 Au CSNC after 3d reactions not only has the max values of the adhesion strength and the viscosity, but also has the highest concentration of anisotropic nanoparticles compared to all the other samples. The comparison among UV-Vis spectra, adhesive and viscosity properties of three nanoadhesive samples highly demonstrated that the shape of the nanoparticles played an important role in the adhesive and viscosity in the nanocomposite adhesive.

The results of mechanical property testing indicated that both nanocomposites with nanoparticle fillers had higher Young's moduli than the matrix without nanoparticles (**Fig. 18**).

This observation confirmed that spherical nanoparticles had a filler effect in reinforcing the mechanical properties of silicone matrix. In determining the size effect of the nano-fillers, we compared the Young's moduli for these two nanocomposites. The results indicated that the silicone nanocomposite with smaller size of polystyrene nanoparticles as fillers has an average value of 432.75 MPa, 38.4 % higher than the silicone with the larger size nanoparticles as fillers.

2.5.2 Surfactant enhanced nanoparticle distribution

As shown in **Fig. 19**, the effect of surfactant on the mechanical performance was obvious in both TiO2 and ZnO nanoparticles as fillers. With the addition of Silwet L-77, fractures were developed in a much later stage for ZnO nanoparticles as fillers than the composite without Silwet L-77. Even no fracture was observed for TiO2 nanoparticle fillers with the addition of Silwet L-77. The moduli of these specimens were also calculated. With Silwet L-77, higher moduli were obtained for both types of nanoparticle fillers compared to the composites without surfactant (**Fig. 19a, b**).

Without Silwet L-77, no obvious increase in Young's modulus was observed, when ZnO nanoparticles were added to the silicone matrix. It should be mentioned that both the TiO2 and ZnO are metal oxides and their sizes vary between 90–200 nm for ZnO nanoparticles, and 50 nm for TiO2 nanoparticles. The moduli measured for these two nano-fillers without surfactant indicated that silicone matrix with TiO2 fillers had a higher modulus than that with ZnO fillers. Similar observations were held in the specimens with surfactant. Since both the ZnO and TiO2 nanoparticles have much higher Young's moduli than the silicone matrix, the difference in Young's modulus of the nanoparticle fillers would not

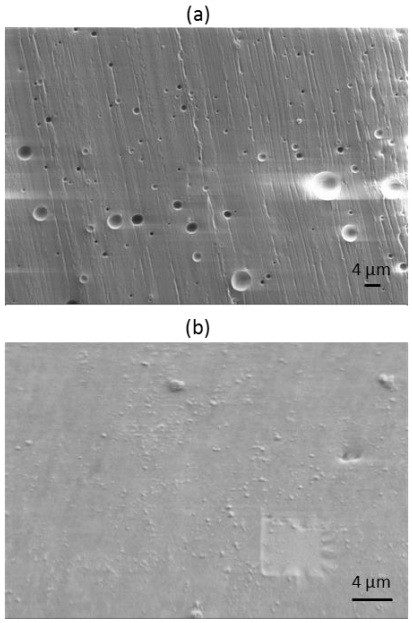

Fig. 20 SEM images of the internal or fracture structures of the TiO_2 nanoparticle-filled silicone matrix with (a) or without surfactant (b). Void growth could be obviously seen from the composites with the addition of surfactant.

cause the observed difference in the nanocomposites, as discussed in later theoretical analysis. Therefore, the observed higher Young's modulus from the composite with TiO2 nano-fillers is likely attributed to the smaller size of the TiO2 nanoparticles. This observation agrees well with the study of size effect of the polystyrene nano-fillers displayed in **Fig. 18**.

It should be noted that the observed difference in Young's modulus between the samples without nano-fillers or surfactant in **Figs. 18** and **19** is attributed to the different ratio of Elastomer Base and Elastomer Curing Agent tested in the experiments.

To examine whether plastic void growth contributes to the enhanced toughness of the matrix, we investigated the internal or fracture structures of the composite using SEM. We checked the internal structure of nanofillers with or without surfactant and compared their plastic void growth. The polymer matrices undergoing investigation were not coated with gold. Thus, passive charge during the SEM scanning prevented us from looking into the structure at the nanoscale.

We could still obtain microscale images of the matrix fractions, as shown in **Fig. 20**. The images indicated that void structures could be easily observed in the matrix with surfactant (**Fig. 20a**), but few could be observed in the matrix without surfactant (**Fig. 20b**). It should be mentioned that these void structures were likely in the microscale, and the existence of nanoscale void structures could not be confirmed. However, the existence of large amount of void structures in the matrix with surfactant implied that the void growth might be another mechanism for the surfactantenhanced modification in addition to assisting in the dispersion of nanoparticles.

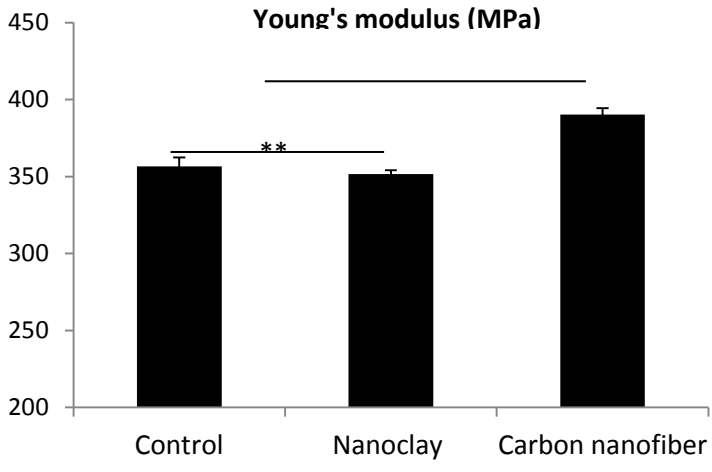

Fig. 21 line showed the process with NH_2 modification and the black line without modification. (b) The moduli of silicone matrix filled with SiO_2 nanoparticles with or without NH_2 modification. The observations from (a) and (b) suggested that NH_2-modificaiton diminished the filler effect of SiO_2 nanoparticles.

Carbon nanofibers were also investigated here to evaluate their potential to enhance mechanical performance of the silicone matrix as fillers. As shown in **Fig. 21**, enhanced mechanical performance could be obtained after the addition of carbon nanofibers. However, compared to the nanoparticles described above, the efficiency is less impressive. Only 9.4% increase in Young's modulus was achieved. The limited increase in Young's modulus could be attributed to the limited distribution of carbon

nanofibers. Carbon nanofibers were difficult to dissolve in deionized water, even with the assistance of Silwet L-77 surfactant. The pre-existed clusters thus prevented the distribution of carbon nanofibers in the Silicone Elastomer Base prior to curing. During the mixing process with the base, a small portion of carbon nanofibers could diffuse in the matrix due to their similar hydrophobicity with the silicone matrix, which then caused the filler effect.

We examined the SiO2 nanoparticles whose surface was coated with amine groups–NH2. After curing, the NH2-modified SiO2 nanoparticles were compared to the nanoparticles without modification. As shown in **Fig. 22**, it was shown that after NH2 modification, the Young's modulus of silicone matrix dropped from 160.6 to 113.2 MPa, a 29.3 % decrease; also the matrix broke at an earlier stage. Through extended research with other biocompatible chemical groups, such as –OH and –COOH, we found that these groups also downgraded the mechanical performance of the nanoparticles as fillers. It is obvious that these coated groups are hydrophilic polar groups. These coated hydrophilic groups, however, might repel with hydrophobic silicone matrix in the interfaces, which thus diminished the filler effect of nanoparticles.

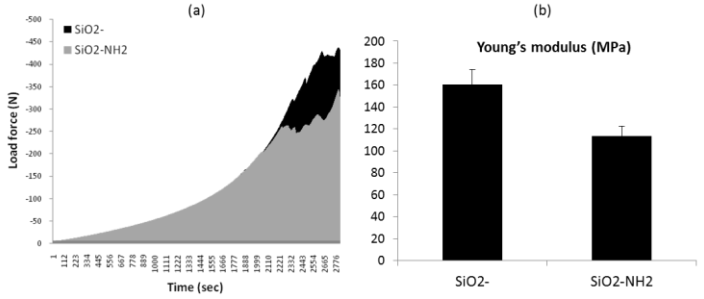

Fig. 22 Effects of surface chemistry on the mechanical effect of nanoparticles as fillers. (a) Mechanical approaching curves for silicone matrix with SiO_2 nanoparticles with or without NH_2 modification. The grey line showed the process with NH_2 modification and the black line without modification. (b) The moduli of silicone matrix filled with SiO_2 nanoparticles with or without NH_2 modification. The observations from (a) and (b) suggested that NH_2-modificaiton diminished the filler effect of SiO_2 nanoparticles.

2.5.3 Theoretical understanding of nanoparticles as fillers in the matrix

In mixtures, the Young's moduli of the composites depend on the Young's moduli of the fillers (**Fig. 23a**), based on the finite element modeling from Abaqus. When the Young's moduli of the fillers are 10 times higher or lower than that of the matrix, further change in Young's modulus of the fillers does not cause additional change of the Young's modulus in the composites. As in this case, the Young's modulus of the silicone matrix is much smaller than those of the fillers used in the current study. This means that the different nanoparticles used, either TiO2 or ZnO, do not affect their filler effect in the silicone matrix, if we are only concerned about the rule of mixtures. In the rule of mixtures, a higher portion of fillers is also expected to enhance the Young's moduli of the composites, as shown in **Fig. 23b, c**.

However, it should be noted that the rule of simple mixtures predicts that the properties of composite materials are independent of the size of inclusions, but are functions of properties of constituents, volume fraction of components, shape and arrangement of inclusions, and matrix–inclusion interfaces. This is true for systems with micron size reinforcement, but may not be right for nanocomposite systems. The effect of nanoparticle fillers depends on many variables, but especially on the relative crystalline or amorphous nature of the polymer matrix and the interactions between fillers and matrix. These experimental results also suggested that the compatibility between the fillers and matrix greatly affected the mechanical properties of nanocomposites.

Although no universal patterns for the behavior of polymer nanocomposites can be concluded, still some models have been developed to explain the trends of observations. The Mori–Tanaka model is used to predict themodulus of particle-modified polymer in some studies, and the model works the best for

relatively high aspect ratios and thus is not proper for use in this case of spherical nanoparticles. The Halpsin–Tsai model predicts the modulus of the composite material as a function of the modulus of the matrix polymer, Em, and that of the filler particles, Ef, aswell as a function of the aspect ratio by the inclusion of a shape factor. The Young's modulus Ec of the composite can be modeled as follows:

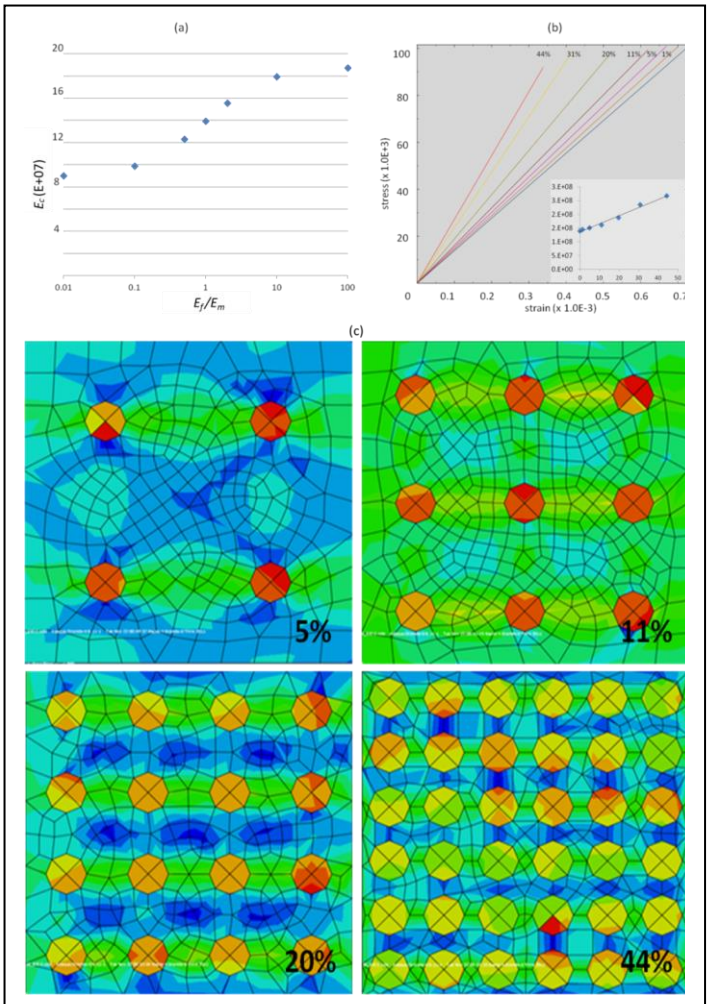

Fig. 23 Predicted moduli of nanocomposites from the finite element modeling. (a) The change of the Young's moduli of the composites (Ec) with the ratio of the Young's moduli between filler (Ef /Em). When the Ef is too high or too low, further change in Ef doesn't cause additional change of Ec. (b) The change of Young's moduli of the composites with the increased concentration of filler particles. A higher concentration of nano-fillers will contribute to a large Ec. (c) Filler effect of four different concentrations of nanoparticles from the finite element modeling analysis. An increased concentration of nano-fillers enhanced the Young's moduli of the composites, which were reflected by the color in the four images. Color with higher wavelength means a lager Young's modulus.

Based on the Halpin–Tsai model, it can be easily seen that with the increase of Vf, the modulus of the composites will increase correspondingly. However, the measured moduli generally lie slightly below the estimated values, which have been proposed due to the imperfect bonding between the nanoparticles and the matrix. The filler effect can be considered further using the Lewise–Nielsen model and the study of McGee and McCullough.

The results from model estimation showed a maximum 30% increase in Young's moduli depending on the concentration of the nano-fillers. Compared to the measured data from **Figs. 18** and **19**, we could see that both models underestimated the moduli of the polystyrene nanocomposites, while they provided proximate prediction when ZnO or TiO2 nanoparticles worked as fillers. One possible reason for the difference observed from polystyrene nanocomposites is that at a relatively low volume ratio, the interface might dominate in determining the filler effect in the nanocomposites, as suggested from other studies. Polystyrene has many phenyl groups which make them extremely hydrophobic, which might draw its strong interaction with the hydrophobic silicon matrix in the interface. These interactions will likely dominate the interface which makes the filler effect more significant than expected.

2.5.4 Synthesis of AuNPs Using Live Shoots

Upon receipt, live ivy shoots were cut to lengths of 15 cm, leaving one attached leaf on the apical end of the stem.

After sterilization and treatment with auxins, four shoots were placed into Magenta GA7 (MAG) boxes and held upright by placing them through holes cut

into the lids. After 24 hours, the boxes were transported to a windowsill, where the nanoparticle synthesis was conducted. To initiate nanoparticles synthesis, aqueous HAuCl4 was added to the 50 ml of water present in the MAG boxes to achieve concentrations of 0, 0.025, 0.05, 0.1, 0.2, 0.5, 1 and 5 mM. The shoots were exposed to these concentrations for 24 hours, before the solution was removed to test for nanoparticle production. After collecting the solution after 24 hours, fresh HAuCl4 solution at the same concentration was added back to the MAG boxes.

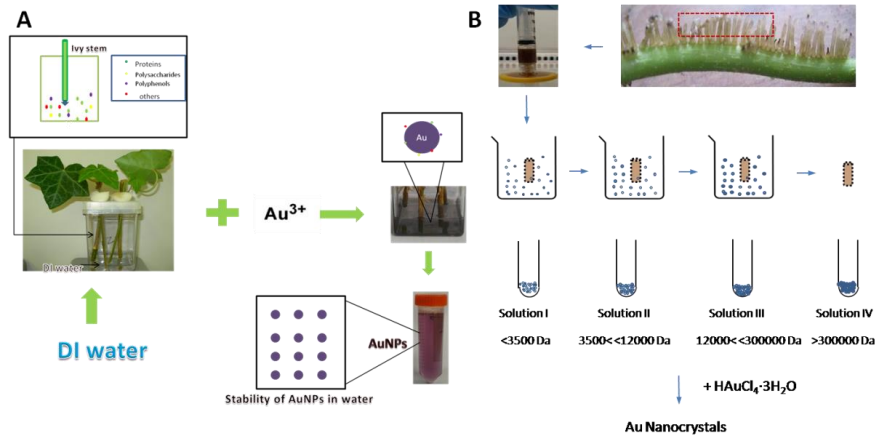

Fig. 24 Schematic diagrams of two different methods used in this study. A), Schematic of the sustainable biosynthesis and stability of AuNP in ivy shoots culture system.$HAuCl_4$ solution was added to the cuture media, and the gold nanoparticles could be collected after 24 hours. And then fresh $HAuCl_4$ solution was added back for sustainable synthesis of AuNPs. B), Procedure for the ivy rootlet extract preparation, separation and gold nanocrystal synthesis. Dialysis tubings with different molecular weight cutoff value (M.W.CO) of 3500 Da, 12,000 Da and 300,000 Da were used to separate different fractions from ivy rootlet extract. And then the four factions were used to synthesize gold nanoparticles.

This method was repeated for the duration of the study. To concentrate any nanoparticles present in the solution, the solution was centrifuged at 14,000 rpm for 10 min. The supernatant was then removed, and DI water was added to the precipitate. This procedure was repeated three times to remove soluble factors present in the solution, including secreted proteins, polysaccharides, and excess HAuCl4. A schematic for this method is shown in **Fig. 24(A).**

2.5.4 Synthesis of AuNPs Using Adventitious Root Extract

Upon receipt, adventitious roots were homogenized in a minimal volume of water, creating a dense solution. This solution was centrifuged at 4,400 rpm for 5 min to remove large tissue debris from the homogenization. The resulting light brown supernatant was then transferred to dialysis tubing with a molecular weight cutoff value (MWCO) of 3.5 kDa, and dialyzed overnight against DI water. After dialysis, the solution outside of the dialysis tubing was collected and labeled as Solution I. The solution remaining in the tubing was then transferred to new tubing and dialyzed at 12 kDa. As indicated above, the solution outside of the tubing was collected and labeled Solution II, followed by a final dialysis through dialysis tubing with a cutoff value of 300 kDa. The final solution outside of the membrane was labeled as Solution III, and the solution remaining in the tubing was labeled Solution IV. Prior to analysis, the extracts were freeze dried and re-suspended in DI water. To synthesize gold nanoparticles from the ivy rootlet extract solutions, 500 l of each solution (I–V) was transferred into a clean microfuge tube and aqueous HAuCl4 was added to a final concentration of 0.5 mM. The mixture was then vortexed, and reacted at room temperature. To concentrate the synthesized gold nanoparticles, the solutions were centrifuged and washed as described above. A schematic for this method is shown in **Fig. 24(B).**

After a few hours, the culture solution changed in color from clear to red, violet, dark purple, and light purple, depending on the concentration of HAuCl4 (insert in **Fig. 25A**). At this point the solution was

removed for analysis of the AuNPs formed during, and fresh HAuCl4 solution was added back to the GA7 boxes. Analysis of the UV-Vis spectra of the solution collected after incubation with HAuCl4 concentrations of 0.025, 0.05, 0.1, 0.2, 0.5 and 1 mM showed a SPB around 550 nm, specific for AuNPs.37 No SPB was present at HAuCl4 concentrations of 0 and 5 mM (**Fig. 25A**). While the SPB appeared at the same absorbance for AuNP forming concentrations, there was a significant difference in the width of the SPB at different concentrations of HAuCl4 solution. To test the sustainability of the AuNP synthesis procedure described above, the HAuCl4 solution was removed and replaced with fresh solution every 24 hours and UV-Vis spectroscopy was conducted on the freshly removed solution to determine if AuNPs were still being produced.

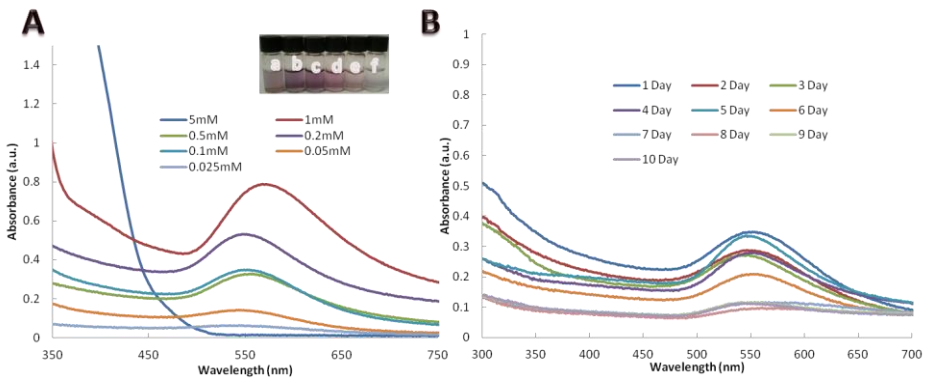

Fig. 25 A. UV-vis absorption spectra of gold nanoparticles synthesized in 0.025, 0.05, 0.1, 0.2, 0.5, 1 and 5mM aqueous $AuCl_4^-$ in ivy culture system in the 1st day. The inset photo showed gold nanoparticles formed with different concentration of aqueous $AuCl_4^-$ (a. 1 mM, b. 0.5 mM, c. 0.2 mM, d. 0.1 mM, e. 0.05 mM, f. 0.025 mM) in ivy culture system. B. UV-vis absorption spectra recorded the gold nanoparticles formation in live ivy culture system, rich with 0.1 mM aqueous $AuCl_4^-$ environment from the 1st day to the 10th day respectively (Each curve experienced 24 hours reaction time).

Fig. 25B shows that at 0.1 mM HAuCl4, AuNPs were formed every 24 hours continuously over a 10 day period. Based on the Beer-Lambert law, the UV-Vis absorbance of a solution is directly proportional to the concentration of the absorbing species in the solution and the path length.

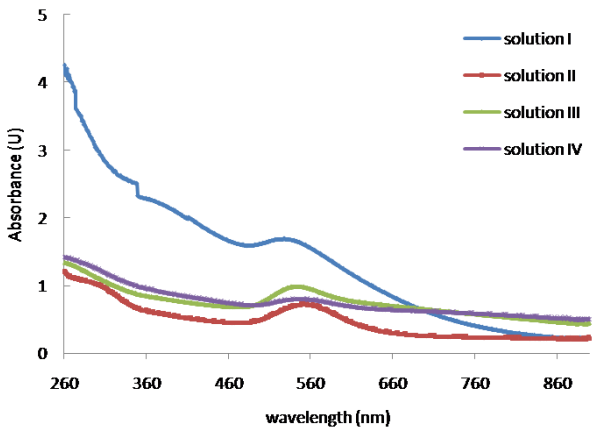

Fig. 26 UV/Vis spectra of gold nanoparticles synthesized by different ivy rootlet extract solutions. Gold nanoparticles from solution I has a larger absorbance value at λ_{max}, indicaitng more gold nanoparticles synhtesized from solution I. Gold nanoparticles from solution III and IV have more absorbance over 720 nm, suggesting more nanoplates or clusteres in the slution III and IV.

In our experiments, the path length was kept constant, thus the concentration of AuNPs in the solution, can be linearly correlated to the absorbance of the AuNP solution. We used this relationship to determine the relative concentration of AuNPs at each time interval, and to calculate the efficiency of the synthesis procedure over time. From the spectral data, the efficiency of AuNP production remained high for the first 5 days, and decreased from day 6–30. Despite the decrease in efficiency, AuNPs could still be obtained from the production system for greater than 30 days, demonstrating the sustainability of this method. The same sustainable property was also observed at lower HAuCl4 concentrations (0.025 mM, 0.05 mM) (**Fig. 25A-B**). In the presence of higher

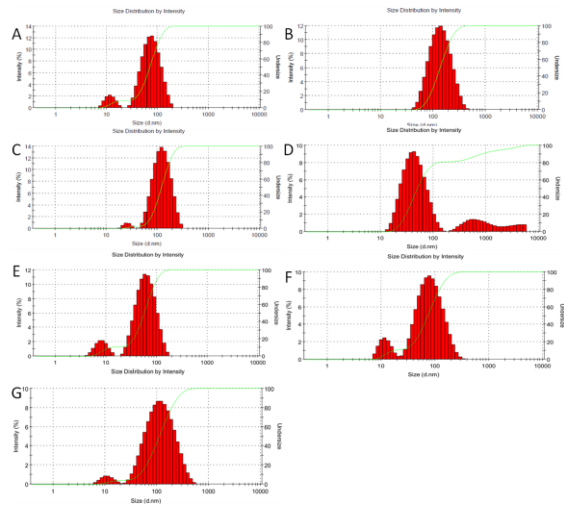

Fig. 27 Size/intensity histograms of gold nanostructures synthesized from 0.1mM (A), 0.5Mm (B), 1mM (C) aqueous $AuCl_4^-$ by live ivy shoots at room temperature. Size/intensity histograms of gold nanoparticles synthesized by different ivy rootlet extract solutions I (D), II (E), III (F) and IV (G).

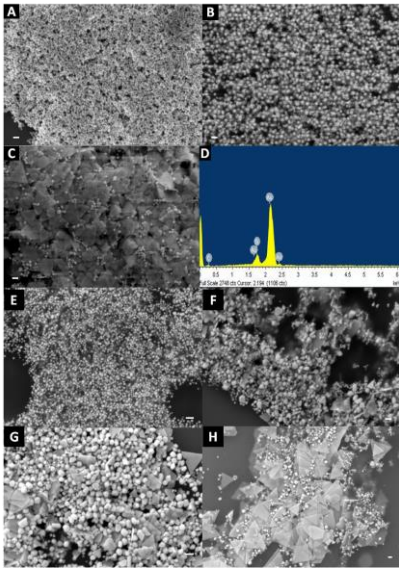

Fig. 30 SEM images of gold nanostructure synthesized in 0.1mM (A), 0.5mM (B), 1mM (C) aqueous $AuCl_4^-$ by live ivy shoots at room temperature, (D) EDX of the treated sample. SEM micrographs of gold nanoparticles synthesized by different ivy rootlet extract solutions I (E), II (F), III (G) and IV (H). (All scale bar= 100nm)

concentrations of HAuCl4 solution (0.5 mM, 1 mM) the decrease in production efficiency was more obvious compared to the lower concentrations, especially at 1 mM HAuCl4. At this high concentration of HAuCl4 some toxicity may occur in the ivy shoots, which decreases the rate of the overall production.

Solutions I–IV were reacted with 0.5 mM HAuCl4 solution at room temperature, as described in the Material and Methods section. A characteristic surface plasmon resonance band (SPR) for gold nanoparticles at 500–600 nm was detected in all four samples (I–IV) (**Fig. 26**), confirming the synthesis of gold nanoparticles in these solutions.

DLS and Zeta potential analysis was used to analyze the size of the AuNPs in solution, and to determine the stability of nanoparticles. DLS of the AuNPs formed using Method One, indicated that the average size of the AuNPs increased from 10 to 300 nm with an increasing concentration of HAuCl4 from 0.025 to 2 mM. This agreed well with the red-shift of the UV-Vis spectra with higher concentrations. The size distribution of gold nanoparticles, formed from 0.1, 0.5 and 1 mM HAuCl4, were measured by DLS.

Based on the Zeta potential analysis, none of the solutions containing the AuNPs, formed using Method One, was stable in water, with zeta potentials ranging from -18.1 to -33.5 mV. This analysis was not surprising, since the AuNPs were observed to sediment from solution, and could easily be centrifuged at a low speeds. The size distributions of AuNPs synthesized using Method Two, were also analyzed by DLS and Zeta potential analysis. AuNPs formed using Solution I and II showed smaller average sizes compared with solution III and IV (**Figs. 27(D–G)**). A significant difference was observed in the Zeta potential of the AuNPs synthesized from the different solutions. Solution I, with a Zeta potential < -30 mV was moderately stable in solution. In solution II, the Zeta potential increased to <-30 mV, suggesting an instability of the AuNPs in solution. The Zeta potential further increased in solution III and IV to larger than -15 mV. Precipitates in these two solutions could be clearly observed, indicating the instability of the AuNPs and the aggregation of these AuNPs.

SEM images of AuNPs synthesized under different conditions are shown in **Fig. 28**. To test whether the AuNPs produced by both methods could be transported into cells for potential biomedical applications, a Cytoviva™ condenser mounted to a Nikon Eclipse

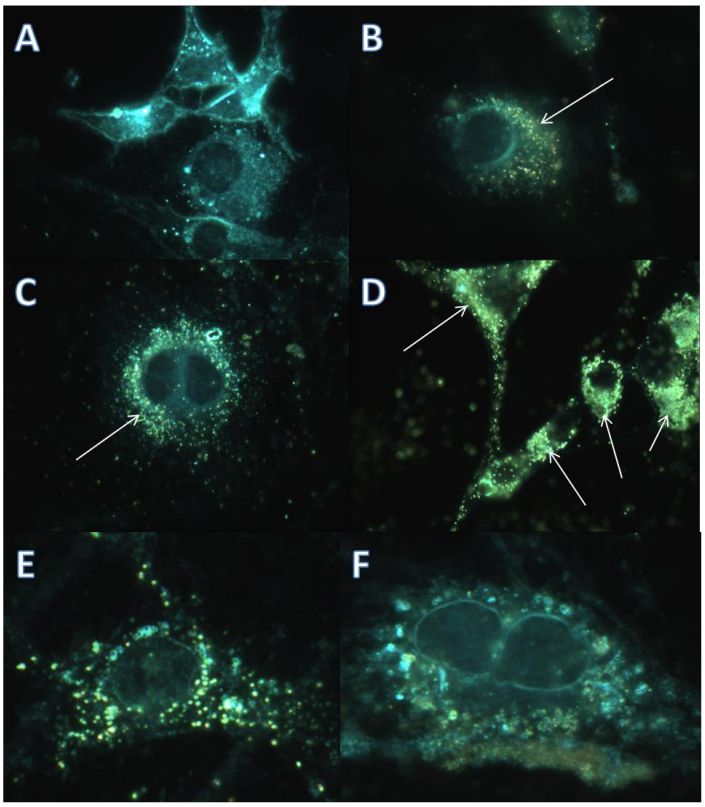

Fig. 29 Dark-field microscopy images of Au NPs synthesized from 0.1 mM $HAuCl_4$ (B), 0.5 mM $HAuCl_4$ (C), 1 mM $HAuCl_4$ (D) in MC3T3 cells respectively. (A) is the control group, without AuNPs. MC3T3 cell incubated with gold nanoparticles from solution II (E), and gold nanocrystals from solution III, IV (F).

microscope was used. Briefly, various AuNPs obtained from both methods were incubated with DMEM containing 10% serum for 24 hours, followed by centrifugation at 14,000 rpm and three washes of PBS. Microscopic analysis showed the internalization of the AuNPs into MC3T3 cells. Using the Cytoviva™ condenser, AuNPs were distinct from organelles due to their scattering properties, which make them appear scarlet or yellow in color (**Fig. 29**). The control group without nanoparticles had no internal particulates, whereas the experimental samples displayed scarlet or yellow nanoparticles. This confirmed that the AuNPs synthesized in this study can be transported across the cell membrane, similar to AuNPs produced by other methods used for cancer therapy. Previously, AuNPs have been proven to have great potential in drug delivery, cancer therapy and bio-imaging applications. It is conceivable that proteins, polysaccharides and other small molecules would provide a robust coating around gold nanoparticles to prevent aggregation.